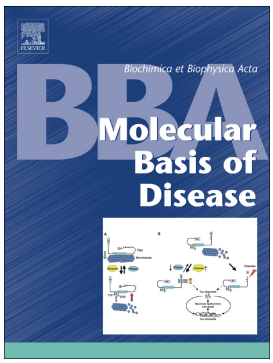


# A long non-coding RNA specifically expressed in early embryos programs the metabolic balance in adult mice

Minzhe Zhu, Qianfeng Wang, Pengxiang Tian, Lu Cheng, Zihao Sun, Qin Hong, Pin Lv, Luzhang Ji, Yang Liu, Qi-Qun Tang, Bo Wen

PII: S0925-4439(20)30336-7

DOI: https://doi.org/10.1016/j.bbadis.2020.165988

Reference: BBADIS 165988

To appear in: *BBA - Molecular Basis of Disease*

Received date: 3 June 2020

Revised date: 18 September 2020

Accepted date: 7 October 2020

Please cite this article as: M. Zhu, Q. Wang, P. Tian, et al., A long non-coding RNA specifically expressed in early embryos programs the metabolic balance in adult mice, *BBA - Molecular Basis of Disease* (2020), https://doi.org/10.1016/j.bbadis.2020.165988

# A long non-coding RNA specifically expressed in early embryos programs the metabolic balance in adult mice

Minzhe Zhu[1#], Qianfeng Wang[1#], Pengxiang Tian[1], Lu Cheng[1], Zihao Sun[1], Qin Hong[1], Pin Lv[1], Luzhang Ji[1], Yang Liu[1], Qi-Qun Tang[1] and Bo Wen[1, 2*]

[1]Key Laboratory of Metabolism and Molecular Medicine, Ministry of Education, Department of Biochemistry and Molecular Biology, School of Basic Medical Sciences, and Institutes of Biomedical Sciences, Fudan University, Shanghai 200032, China

[2]State Key Laboratory of Genetic Engineering, Collaborative Innovation Center of Genetics and Development, Fudan University, Shanghai 200438, China

[#]Contribute equally

*Correspondence: Email, bowen75@fudan.edu.cn; Tel：86-21-54237505

**ABSTRACT**

Many Long non-coding RNAs (lncRNAs) are specifically expressed in early embryos, but the physiological functions of most of them remain largely unknown. Here, we show that deficiency of *lncenc1*, an early embryo-specific lncRNA, altering glucose and lipid balance in adult mice. Newly weaned *lncenc1*-deficient mice prefer to use lipids as a fuel source. When mice were fed a normal chow diet (NCD), glucose intolerance and insulin resistance were observed in adult *lncenc1*-deficient mice. Under high-fat diet (HFD) conditions, however, *lncenc1*-deficient mice became healthier and could resist food-induced obesity and metabolic disturbances. Furthermore, AKT/mTOR-regulated lipogenesis in liver was reduced in *lncenc1*-deficient mice fed a HFD. MEFs lacking *lncenc1* showed impaired glycolysis and lipogenesis, suggesting that the metabolic defects may already exist in embryos. Our study demonstrated the essential roles of *lncenc1* in adult metabolism, providing experimental data that support the "fetal origin" of adult metabolic disorders.

**Keywords** Fetal origin; Glycolysis; Lipogenesis; Long noncoding RNAs; Metabolic homeostasis

**Abbreviations :** lncRNA, Long non-coding RNA; NCD, Normal chow diet; HFD, High fat diet; BAT, Brown adipose tissue; eWAT, Epididymal white adipose tissue; iWAT, Inguinal white adipose tissue; MEF, Mouse Embryonic Fibroblast; mESC, mouse embryonic stem cell; GTT, Glucose tolerance test; ITT, insulin tolerance test; HOMA-IR, homeostasis model assessment of insulin resistance; FISH, Fluorescence in situ hybridization; TRIGL, Triglyceride Level; HDL-C, High cholesterol level; CHOL, Cholesterol; LDL-C, Low cholesterol level; ALT, Alanine aminotransferase; AST, Aspartate transaminase; RER, Respiratory exchange rate; MRI, Magnetic Resonance Imaging; mTOR, Mammalian target of rapamycin; AKT, Protein kinase B; AMPK, AMP-activated protein kinase; Glut4, Glucose transporter type 4; Hk2, Hexokinase

type II; Gpi, Glucose-6-phosphate isomerase; Pfk, ATP-dependent 6-phosphofructokinase; Aldo, Fructose-bisphosphate aldolase; Tpi1, Triosephosphate isomerase; Gapdh, Glyceraldehyde-3-phosphate dehydrogenase; Pgk1, Phosphoglycerate kinase 1; Eno, enolase; Pgam, Phosphoglycerate mutase; Pkm, Pyruvate kinase; Ldha, L-lactate dehydrogenase A chain; CD36, Long -chain fatty acid transporter; Fasn, Fatty acid synthase; Acc1, Acetyl-CoA carboxylase 1; Srebp1-c, Sterol regulatory element-binding protein 1; Pparγ, Peroxisome proliferator-activated receptor gamma; Gpam, Glycerol-3-phosphate acyltransferase 1; Scd1, Acyl-CoA desaturase 1; C/EBPa, CCAAT/enhancer-binding protein

## 1. INTRODUCTION

Normal energy metabolism is characterized by switches between alternative fuels, i.e., glucose and lipid, according to physiological and nutritional circumstances [1]. However, chronic overnutrition could impair this energy homeostasis and cause metabolic syndrome, which has become a global epidemic and increases the risk for type 2 diabetes mellitus, cardiovascular diseases, and non-alcoholic fatty liver disease [2, 3]. The incidence of metabolic syndrome in the world is 10–40%, indicating that it is a serious threat to human health [4]. The “fetal origins of adult disease” hypothesis was proposed by Dr. Barker from the MRC Institute of Environmental Epidemiology in 1989. According to this hypothesis, metabolic reprogramming caused by malnutrition or genetic mutations during embryonic development determines long-term adult phenotype abnormalities [5]. Studies have shown that genetic polymorphisms of the *IGF2BP2* and *PPAR-γ2* genes in the Dutch population born during the famine of 1944–1945 are associated with the symptoms of adult disease caused by fetal malnutrition [6, 7]. Although it is difficult to rule out maternal effects in malnutrition research, this may be accomplished using genetic studies in embryos. For example, fetal deficiency of *Lin28a* and *Lin28b* in mouse embryos can cause aberrations in growth and glucose metabolism in adults [8].

However, studies on this subject are still limited in number, because most of the genes involved in metabolism are often widely expressed and have an impact on the development of adult tissues. By gene editing methods, it is possible to temporarily downregulate target genes during embryonic development, but these experiments are challenging to perform. Therefore, genes that are specifically expressed in embryos are ideal targets for studying the fetal origin of metabolic reprogramming.

LncRNAs are a unique class of transcripts; they are over 200 nt long and do not have protein coding potential. Like mRNA, most lncRNAs are transcribed by RNA polymerase II and undergo splicing, capping, and polyadenylation [9, 10]. Interestingly, lncRNAs exhibit tissue-specific and highly regulated expression patterns, and they are involved in diverse biological processes. Functional studies have indicated that multiple lncRNAs control metabolic tissue development and function, including hepatic metabolism, adipogenesis, islet function, and energy balance [11-13]. Expression profiling studies and gain- or loss-of-function approaches in cell-based *in vitro* systems have uncovered important roles for many lncRNAs specifically expressed in pluripotent stem cells (PSCs) [14-16]. Yet, the *in vivo* physiological functions of early embryo-enriched lncRNAs remain elusive.

The overarching question of our research is whether lncRNAs can regulate metabolism in the embryo and thereby determine long-term adult energy homeostasis, and if so, by which mechanisms. In a previous study, we showed that *lncenc1*, a lncRNA specifically expressed during embryonic development, regulates the expression of glycolytic genes through interacting with hnRNPK and PTBP1 in mouse embryonic stem cells (mESCs) [17]. The mouse lacking *lncenc1* could be an ideal model for studying the fetal origin of metabolic abnormalities. We used two gene-editing strategies to construct global knockout strains. We found that, due to the impaired glycolytic and lipogenetic activity in embryos, the glucose and lipid balance is reprogrammed in *lncenc1*-knockout mouse.

## 2. METHODS

### 2.1. Animals and diets

All of the mice were generated by Shanghai Biomodel Organism Co., Ltd. Mice were maintained in colony cages at an environmental temperature of 22±1°C and humidity of 45±10% under a 12/12 hr light/dark cycle. All of the mice had free access to water, and food was only withdrawn if required for an experiment.

We used two knockout strategies to generate *lncenc1*-deficient mice. The first strategy was to integrate a premature polyadenylation cassette in the middle of the first exon (*lncenc1*$^{3A/3A}$), resulting in early termination of the transcript without long-range genomic disruption. The second strategy was to delete exon 3 of the *lncenc1* gene (*lncenc1*$^{\Delta E3/\Delta E3}$), which is a straightforward approach and leaves no residual transcript of the major exon [18]. Only male mice were used during this study. Six-week-old *lncenc1*$^{3A/3A}$ mice, *lncenc1*$^{\Delta E3/\Delta E3}$ mice, and their wild-type littermates were subjected to NCD (60% energy from carbohydrates, SLRC) or HFD (60% energy from fat, Research Diets). Mice were maintained on HFD for 20 weeks, and body weights were recorded every week. Body composition was assessed using an NMR analyzer (Bruker). Moreover, energy expenditure, oxygen consumption, food intake, and physical activity were measured with CLAMS (Columbus Instruments, Columbus, OH, USA). At the end of the experiment, iWAT, eWAT, BAT, and liver tissue were collected by dissection and snap-frozen in liquid nitrogen for protein and RNA analysis or fixed in 4% paraformaldehyde for immunohistochemistry. Ethical approval was obtained by the Committee for Animal Care and Experimental Use of the Fudan University School of Basic Medical Sciences (no. 20160225-059). All of the animal studies were approved by the Institutional Animal Care and Use Committee (IACUC) of Fudan University and were in accordance with NIH guidelines.

### 2.2. RNA extraction and reverse transcription (RT)-qPCR

Total RNA was isolated from tissues and cultured adipocytes using TRIzol lysis reagent (Invitrogen). Complementary DNA was synthesized from 1 μg total RNA using PrimeScript RT Master Mix (TaKaRa) with random primers following the manufacturer's instructions. Real-time qPCR assays were run in duplicate on a LightCycler 480 instrument (Roche) using 2× Sybr Green PCR Master Mix (Roche Applied Science, Indianapolis, IN). All of the relative mRNA expression levels were calculated by the ΔΔCt method with *Actb* as the invariant control. Primers used are listed in Table S1.

**2.3. Western blotting**

The Western blotting experiments were conducted as described [17]. Proteins were extracted from tissue samples (after snap freezing) or from cultured cells in lysis buffer. Antibodies: mTOR (CST Cat#2933), Ser2448-mTOR (CST Cat#5536), AKT (CST Cat#4691), Ser473-AKT (CST Cat#4060), Thr308-AKT (CST Cat#13038), AMPK alpha (CST Cat#5831), Thr172-AMPK alpha (CST Cat#50081), TPI1 (Proteintech Cat# 10713-1-AP), ALDOC (Proteintech Cat#14884-1-AP), PFKP (Proteintech Cat#13389-1-AP), ACTB (Proteintech Cat#60008-1-AP), Foxo1( HUABIO Cat#ET1608-25), p-Foxo1(Beyotime Cat#AF605).

**2.4. RNA fluorescence in situ hybridization (FISH)**

RNA FISH for the detection of *lncenc1* and Ppib (positive control) was performed using RNAscope (Advanced Cell Diagnostics Inc., Hayward, CA 323100), according to the protocol provided by the manufacturer.

**2.5. The measurement of glucose uptake and lactate production**

The same amount of MEF from two strains were seeded on a well of 12-well plates. After 24 hours, cultured medium was collected for glucose and lactate measurement, using the Cobas C311 Chemistry Analyzer (Roche), according to the manufacturer's

instruction. The intracellular glucose consumption and lactate production were calculated by the concentration differences between cultured medium and the blank medium.

### 2.6. Cell culture

Mouse ESC line (E14TG2a) were cultured in 2i /LIF conditions as described [19]. The shRNA-based knockdown experiments were conducted as described previously [20].

### 2.7. MEF differentiation and treatment

Mouse Embryonic Fibroblasts (MEFs) were isolated at E12.5 as described [21]. Adipogenesis of MEFs was performed as previously described [22]. Two days after reaching confluence (designated day 0), MEFs were induced with rosiglitazone and MDI cocktail.

### 2.8. Oil red O staining

Oil Red O (0.7 g) was dissolved in 200 ml of isopropanol and filtered with 0.22-μm filters. The solution was diluted with water (3:2). The differentiated adipocytes were washed twice with cold PBS and fixed with 3.7% formalin for 15 min, stained with Oil Red O for 4h at room temperature, washed twice with $ddH_2O$, dried at room temperature, and then visualized and photographed.

### 2.9. Histological analysis and HE staining

Tissues were fixed with 3.7% paraformaldehyde at 4°C overnight, embedded in paraffin, sectioned, and stained with HE following standard procedures. Immunohistochemistry experiments were performed by Shanghai Rui Yu Biotechnology Co., Ltd.

### 2.10. Glucose tolerance test (GTT) and insulin tolerance test (ITT)

For the GTT, mice were placed in a clean cage with water and injected with D-glucose (2 mg/g body weight, intraperitoneally) after an overnight fasting (16 h). Tail vein blood glucose levels were measured at 6 time points after injection. For the ITT, mice were injected with insulin (0.75 mU/g body weight, intraperitoneally) after fasting for 4 h, and tail vein blood glucose levels were measured at 6 time points after injection.

### 2.11. Serum parameter measurements

Blood samples were collected by the retro-orbital bleeding method using heparinized capillary tubes. Blood samples were then transferred to Eppendorf tubes and centrifuged within 30 min of collection to separate plasma. Glucose, triglyceride, cholesterol, LDL, HDL, ALT, and AST levels were assayed using an automatic biochemical analyzer (cobas c 311, Roche).

### 2.12. Body composition measurements

Live mice were placed into a thin-walled plastic cylinder, and body composition tests were carried out by an NMR analyzer (Bruker) following the manufacturer's instructions.

### 2.13. Metabolic studies (CLAMS)

Four-week-old mice were maintained individually in a metabolism chamber (Comprehensive Lab Animal Monitoring System, CLAMS) with free access to food and water for 72 hours. Mice were housed for 24 hours for adaptation. Metabolic parameters, i.e., energy expenditure, $O_2$ consumption, $CO_2$ production, RER, and total locomotor activity, were recorded at 10 min intervals in a standard 12/12 hr light/dark cycle at 25°C. The RER is the ratio of carbon dioxide production to oxygen consumption ($VO_2$), i.e., RER = $VCO_2/VO_2$. Energy expenditure was calculated as the product of the calorific value of oxygen/carbon dioxide and the consumption ($E = 3.815 \times VO_2 + 1.232 \times VCO_2$) [23].

### 2.14. Statistical analysis

The data of calculation cell size are expressed as mean value ± SD. All the other data are expressed as mean value ± SEM. All of the Fig.s were generated and statistical analyses were carried out using GraphPad Prism 7.0; n indicates the number of animals per group or number of independent experiments. The statistical significance of differences between two groups was assessed using the two-tailed Student *t*-test. The level of significance was set at $*P < 0.05$; $**P < 0.01$; $***P < 0.001$.

### 2.15. Liver transcriptomics

For reads mapping, paired-end 150-bp reads were mapped to the mouse mm10 reference assembly (GRCm38, patch 3) with hisat2 (version 2.1.0) [24], using default parameters. Only reads of high mapping quality (mapQ > 20) that aligned to unique locations were retained with NH:i:1 tag. Unique SAM files were converted to BAM files and then sorted and indexed by samtools (version: 1.7) [25]. The GENCODE M21 GTF was used as annotation reference. For gene expression level analysis, we used the Fragments Per Kilobase of transcript per Million fragments (FPKM), which was calculated with StringTie version 1.3.6 [26]. For differential gene expression analysis, raw count tables for GENCODE M21 gene models were quantified using HTSeq version 0.6.1 [27]. Differential expression statistics were obtained with DESeq2 [28] R package version 1.22.2, with default settings, except for the FDR threshold (reduced to a more stringent 0.05) and the absolute value of log2(fold change) > 1.For visualization on IGV, the BIGWIG files from forward and reverse strands were separately generated and normalized using RPGC by bamCoverage with deeptools 3.1.0 [29]. GO enrichment analysis on gene sets was performed on the DAVID [30] website, and biological process terms were ranked based on Benjamini-corrected *P*-values.

### 2.16 Data availablility

Liver RNA-seq data files have been deposited at the Gene Expression Omnibus (www.ncbi.nlm.nih.gov/geo) with accession number GSE135314. Enter token "qdazgmyqnzgjzmn" into the box.

## 3. RESULTS

### 3.1. Generation of *lncenc1*-deficient mice

To investigate the *in vivo* gene expression pattern of *lncenc1*, we first measured the expression levels of *lncenc1* in different murine tissues. As expected, *lncenc1* is highly expressed in mouse blastocyst stage embryos (E3.5) compared to other examined tissues (Fig. 1A). During early development, the expression levels rapidly decreased after implantation according to published RNA-seq data [31, 32] (Fig. 1B). Furthermore, RNA FISH experiments indicated that transcripts of *lncenc1* are detected in cells from the inner cell mass with high expression level of *Pou5f1*, a classic pluripotency marker (Fig. 1C). These data indicate that *lncenc1* expresses specifically in early developmental stages *in vivo*.

To explore the biological functions of *lncenc1*, we generated two *lncenc1*-knockout models: *lncenc1*$^{3A/3A}$ and *lncenc1*$^{\Delta E3/\Delta E3}$ (see Methods; Fig. 1D and Fig. S1A-B). In both models, we were able to successfully abolish *lncenc1* expression in blastocysts (Fig. 1E) and major metabolic tissues in adult mice (Fig.S1C). Functional experiments were performed mostly in *lncenc1*$^{3A/3A}$ mice, because of the smaller genomic disruption, and the experiments in *lncenc1*$^{\Delta E3/\Delta E3}$ mice were performed to further confirm the results. *lncenc1*$^{wt/wt}$ and *lncenc1*$^{+/+}$ mice were control littermates for *lncenc1*$^{3A/3A}$ and *lncenc1*$^{\Delta E3/\Delta E3}$ mice, respectively.

We first observed the birth rate, sex ratio, and birth weight of different genotypes. Both *lncenc1*$^{3A/3A}$ and *lncenc1*$^{\Delta E3/\Delta E3}$ mice were viable at birth, with a birth rate of about 22% (39/181) and 24% (24/99), which are similar to the expected Mendelian ratio (25%), indicating no embryonic lethality occurred in knockout embryos. In addition,

there were no significant differences in sex ratio and birth weight between different genotypes (Fig. 1F-G, Fig. S1D-E). Mice showed no gross abnormalities and were viable to more than one year of age. Therefore, *lncenc1* is not required for embryonic development and viability.

### 3.2. *lncenc1* deficiency drives a metabolism change at weaning

Since we had shown *lncenc1* impairs the capacity to perform glycolysis in mESCs, we wondered whether *lncenc1* deficiency also have influence on metabolism *in vivo.* The *lncenc1*$^{3A/3A}$ mice exhibited slight glucose intolerance compared to wildtype littermates at weaning (4 weeks) (Fig. 2A), and fasting insulin levels were also slightly elevated (Fig. 2B).

To further analyze the fuel utilization of *lncenc1*$^{3A/3A}$ mice at this stage, we performed the metabolic cage experiments. Notably, *lncenc1*$^{3A/3A}$ mice showed a moderate decrease in respiratory exchange ratio (RER) during both the day and the night (Fig. 2C), indicating a compensatory upregulation of fat utilization. Meanwhile, *lncenc1*$^{3A/3A}$ mice had higher energy expenditure, as evidenced by the higher volume of consumed oxygen ($VO_2$) (Fig. 2D), with unaltered total daily food consumption or activity between the two cohorts (Fig. 2 E-F). We also measured several genes related to energy regulation in brown adipose tissue. *Ucp1*, *Cidea* and *Elovl3* were slightly up-regulated under NCD (Fig.S2A), further confirming that *lncenc1*$^{3A/3A}$ mice had higher energy consumption. In summary, *lncenc1*$^{3A/3A}$ mice at weaning exhibit metabolism changes, including a trend for glucose intolerance, a shift in fuel utilization and the higher energy consumption.

### 3.3. *lncenc1*-deficient mice have impaired glucose homeostasis under NCD conditions

We further explored the influence on glucose homeostasis in the adult mice. Normal chow diet (NCD), with glucose as the main energy source, was fed to

*lncenc1*$^{3A/3A}$ mice and their littermate controls. To assess the kinetics of weight gain in these animals, we measured body weight every week, starting at 6 weeks age. On an NCD, body weight and length were similar between *lncenc1*-deficient mice and their littermate controls over 26 weeks of life (Fig. 3A-B). And the food consumption between the two strains also had no difference (Fig. 3C). To characterize how *lncenc1* deficiency affects glucose homeostasis, we performed the Glucose tolerance test (GTT) and insulin tolerance test (ITT), classic metabolic tests used for the characterization of whole-animal glucose metabolism, on adult mice (age above 12 weeks). Consistent with the results at weaning, *lncenc1* depletion significantly impaired glucose tolerance, as indicated by GTT (Fig. 3D). Moreover, their insulin sensitivity was also significantly reduced as showed by ITT (Fig. 3E), while serum levels of insulin were similar between WT and *lncenc1*$^{3A/3A}$ mice (Fig. 3F). These results show that *lncenc1*-deficient mice clear blood glucose less efficiently.

Furthermore, *lncenc1*$^{3A/3A}$ mice had less epididymal white adipose tissue (eWAT), while the weight of inguinal white adipose tissue (iWAT), brown adipose tissue (BAT) and liver did not change (Fig. 3G-H). Hematoxylin and eosin (H&E) staining and the quantification showed that the cell sizes of eWAT in *lncenc1*$^{3A/3A}$ mice were statistically smaller than those in WT mice, while the cell sizes of iWAT and BAT were similar between the two strains (Fig. 3I-J). Moreover, the liver appearance and the cell morphology of liver were not different between the two strains according to H&E (Fig. 3K, M). Also, the triglyceride (TG) and cholesterol (CHO) content didn't change, consistent with the results of Oil Red O staining (Fig. 3L-M).

Skeletal muscle tissue exhibits high glycolytic activity and accounts for 60%–80% of the increase in glucose metabolism in response to insulin [33, 34]. In order to elucidate the mechanisms underlying glucose intolerance and insulin resistance, we investigated the effects of *lncenc1* knockout on skeletal muscle tissue. We examined mRNA expression levels by RT-qPCR in muscle of *lncenc1*$^{3A/3A}$ mice. The expression levels of all glycolysis genes tend to decline, especially phosphofructokinase (*Pfkp*)

and aldolase isozymes A and C (*Aldoa*, *Aldoc*), which were significantly downregulated (Fig. 3N). PFKP and ALDOA/C, glycolytic key enzymes, control glycolysis activity. PFKP catalyzes the phosphorylation of fructose-6-phosphate (F6P) to fructose-1,6-bisphosphate (FBP). FBP is a sensor of glucose availability and represses AMP-activated protein kinase (AMPK) activation. Aldolases also act as a sensor of falls in glucose availability and transmit the signal to AMPK [35]. Correspondingly, *lncenc1*$^{3A/3A}$ mice exhibit increased AMPK phosphorylation in muscle tissue (Fig. 3O). Once activated, AMPK would promote alternative catabolic pathways to generate ATP, such as fatty acid oxidation. Consistently, we found an evaluated trend for genes of energy expenditure (*AP2*, *Ucp1*) and fatty acid metabolism (*Atgl, Hsl, Ppara* and *Cpt1a*) in eWAT and liver respectively (Fig.S2B-C). We also detected a decreased RER in adult *lncenc1*$^{3A/3A}$ mice (Fig. S2D), suggesting an increased fat oxidation capacity. The physical activity of the two strains mice was similar (Fig. S2E).

To further confirm the results obtained in *lncenc1*$^{3A/3A}$ mice, we also analyzed some phenotypes of *lncenc1*$^{\Delta E3/\Delta E3}$ mice under the NCD condition. Although the body weight was similar between *lncenc1*$^{\Delta E3/\Delta E3}$ and their littermate controls (Fig. S3A), the *lncenc1*$^{\Delta E3/\Delta E3}$ *mice* had impaired insulin sensitivity and glucose intolerance under NCD (Fig. S3B-C). The weight of liver was no difference, however, the weights of all three fat pads in *lncenc1*$^{\Delta E3/\Delta E3}$ mice were reduced (Fig. S3D-E). The cell sizes of all three fat pads in *lncenc1*$^{\Delta E3/\Delta E3}$ mice were statistically decreased based on the H&E staining and quantification (Fig. S3F-G). Furthermore, the expression of glycolysis genes in *lncenc1*$^{\Delta E3/\Delta E3}$ mice were down-regulated (Fig. S3H). Therefore, the phenotypes of these two knockout strains were largely similar. However, the reductions of fat weights and cell sizes were stronger in *lncenc1*$^{\Delta E3/\Delta E3}$ mice, probably because the complete deletion of exon 3 is more efficient to eliminate the expression of *lncenc1*.

Together, these results indicate that adult *lncenc1*-deficient mice exhibited

defective glycolysis and impaired homeostasis, such as glucose intolerance and insulin resistance, during NCD feeding. Moreover, inefficient glycolysis resulted in increased energy expenditure on fatty acid and lower adiposity.

### 3.4. *lncenc1*-deficient mice resist diet-induced obesity and liver steatosis

According to the “thrifty genotype” hypothesis, humans have “evolutionary physiology,” i.e., our bodies tend to preserve body fat to increase future survival chances [36]. However, the availability of calories is almost unlimited in modern society, which has caused a lot of people to gain excessive weight. Since *lncenc1*-deficient mice prefer to use lipids as fuel at weaning and loss-of-function experiments with several glycolytic genes (*Ldha, Aldoa,* and *Tpi1*) showed fat or weight loss phenotypes in mice according to the MGI database, we next explored the effects of *lncenc1* deficiency in the case of high-fat overnutrition.

Six-week-old *lncenc1*$^{3A/3A}$ male mice and their littermate controls were fed HFD (60% energy from fat) for 20 weeks, and body weight was measured every week. Notably, *lncenc1*-deficient mice did not gain as much weight as their littermate controls (Fig. 4A-B). The body weight of *lncenc1*$^{3A/3A}$ mice was 14% lower than that of wild-type littermates. Different mouse strains consumed equivalent amounts of food, indicating that the reduction in weight was not due to a reduction in food uptake (Fig. 4C). Body composition analysis using magnetic resonance imaging (MRI) at 8, 12, 19-week of feed age revealed that *lncenc1*$^{3A/3A}$ mice accumulated less fat mass, whereas their gains in lean mass were similar to those observed in wild-type mice under HFD conditions (Fig. 4D). These changes in fat mass were confirmed after mice were sacrificed. After 20 weeks of HFD treatment, the weight of the iWAT, eWAT, and BAT decreased 30.09%, 17.75%, and 38.13% respectively, compared with wild-type littermates (Fig. 4E-F). Furthermore, the H&E staining and the quantification of cell sizes of the three fat pads revealed that the diameters of dipocytes in *lncenc1*$^{3A/3A}$ mice were significantly decreased (Fig. 4G-H). HFD-fed wild-type mice

developed acute hepatomegaly with a 35.5% increase in liver weight compared to HFD-fed *lncenc1*$^{3A/3A}$ mice (Fig. 4I). The TG and CHO content in liver were significantly down-regulated in *lncenc1*$^{3A/3A}$ mice under HFD condition (Fig. 4J). These data were consistent with histologically evidence of hepatosteatosis according to H&E and Oil Red O staining, while HFD-fed *lncenc1*$^{3A/3A}$ mice had minimal or no signs of steatosis (Fig. 4K).

We also fed *lncenc1*$^{\Delta E3/\Delta E3}$ mice with HFD for 20 weeks and the phenotypes, including body weights, fat tissue weights, adipocytes sizes and liver pathologies were highly consistent with those observed in *lncenc1*$^{3A/3A}$ mice (Fig. S4A-F).

In summary, these results demonstrate that *lncenc1*-deficient mice were protected from HFD-induced obesity and liver steatosis.

### 3.5. *lncenc1*-deficient mice have improved metabolic parameters under HFD

HFD is a well-established metabolic stress that can lead to abnormal obesity in mice and produce metabolic disorders, such as insulin resistance and liver steatosis [37]. Under HFD conditions, *lncenc1*-deficient mice did not increase their body weight as much as the wild-type mice did and showed alleviated liver steatosis. Next, we examined whether *lncenc1* deficiency could protect mice from diet-induced metabolic disorders. As anticipated, *lncenc1*$^{3A/3A}$ mice had lower fasting glucose levels after HFD treatment (Fig. 5A). Consistently, the fasting serum insulin levels and the insulin resistance index HOMA-IR of *lncenc1*$^{\Delta E3/\Delta E3}$ mice were significantly lower compared with wild-type littermates (Fig. 5B). To further examine this concept, we next performed the GTT and ITT. *lncenc1*$^{3A/3A}$ mice were significantly protected from HFD-induced glucose intolerance compared with their wild-type littermates (Fig. 5C). The ITT assay showed that *lncenc1* deficiency improved insulin sensitivity under HFD conditions (Fig. 5D). These results demonstrate that HFD can compensate for the inefficient glucose uptake observed in *lncenc1*$^{3A/3A}$ mice fed NCD and that *lncenc1*$^{3A/3A}$ mice are protected from HFD-induced glucose intolerance and insulin resistance.

HFD-induced obesity is ultimately accompanied by serum dyslipidemia. *lncenc1*$^{3A/3A}$ mice showed alleviated serum low-density lipoprotein cholesterol (LDL-C), and a tendency to hypocholesterolemia (CHO2I) and lower serum high-density lipoprotein cholesterol (HDL-C) during fasting (Fig. 5E). Similarly, fasted serum levels of CHO2I, HDL-C and LDL-C in *lncenc1*$^{\Delta E3/\Delta E3}$ mice were significant decreased compared to wildtype littermate controls (Fig. 5F). The liver takes up circulating fatty acids, which are the main source of liver triglycerides [38]. We have shown that TG content in the liver of *lncenc1*-deficient mice was significantly reduced under HFD stimulation (Fig. 4J). Accordingly, the triglyceride serum levels during fasting were significantly higher in *lncenc1*-deficient mice on HFD than those of their wild-type littermates (Fig. 5G). The phenotypes of *lncenc1*-deficient mice were similar to the *Dicer* fat-specific KO mice, which were also lean but with hypertriglyceridemia [39]. To explain the reason for the increase of serum TG content, We detected the transcriptional expression of lipoprotein lipase (Lpl) in muscle and fat (eWAT), and found that the expression of Lpl in muscle and fat (eWAT) decreased in lncenc1-deficient mice, especially significantly reduced in fat (eWAT) tissues, compared to the littermate controls (Fig. 5H). The defect of Lpl in the muscle and fat in lncenc1-deficient mice could provide a plausible mechanism to explain why lncenc1-deficient mice are hypertriglyceridemic in the fasted state. To examine whether liver steatosis was alleviated, we next examined whether *lncenc1*-deficient mice had improved liver parameters. The alanine transaminase (ALT) levels of HFD-fed *lncenc1*$^{3A/3A}$ and *lncenc1*$^{\Delta E3/\Delta E3}$ mice were significantly lower than those of wild-type mice (Fig. 5I-J). In summary, we conclude that the absence of *lncenc1* results in improved metabolic parameters under overnutrition conditions.

### 3.6. AKT/mTOR-regulated lipogenesis is repressed in *lncenc1*-deficient mice

The liver plays a central role in balancing glucose, lipid and amino acid uptake, managing whole-body metabolism and maintaining metabolic homeostasis [37]. To

explore the molecular mechanisms of *lncenc1* deficiency-induced protection against hepatic steatosis, we performed RNA-seq analysis on the liver of HFD-fed wild-type and *lncenc1*$^{3A/3A}$ mice. Differential expression analyses were conducted using DESeq2 (Methods for details; Table S1 for results). Between *lncenc1*$^{3A/3A}$ and wild-type mice, 407 genes were downregulated and 601 genes were upregulated significantly (adjusted $P \leq 0.05$) on HFD (Fig. 6A).

The genotype-specific differences in gene expression may explain genotype-specific metabolic changes. Functional annotation of transcripts that were differentially expressed between *lncenc1*$^{3A/3A}$ and wild-type livers revealed that many genes were involved in lipid metabolism, i.e., genes involved in lipid intake (*Cd36*, *Apoe*, and *Fabp1/2*), fatty acid oxidation (*Acadm, Hadh, Ehhadh,* and *Acaa1b*), *de novo* lipogenesis (*Fasn*, *Scd1/2,* and *Elovl5*), triglyceride synthesis (*Mogat1, Gpam, Gpat2,* and *Agpat4*), and triglyceride storage (*Plin2, Cidea,* and *Vldlr*) were downregulated in *lncenc1*$^{3A/3A}$ under HFD conditions (Fig. 6B). The changes in their expression levels correlated with alleviated liver steatosis and increased circulating TG observed in *lncenc1*-deficient mice. Many genes involved in cholesterol and sterol synthesis were downregulated, which may explain the low cholesterol levels in *lncenc1*- deficient mice.

Most genes involved in liver lipogenesis were significantly downregulated in *lncenc1*- deficient mice, including master regulators, such as *Srebp1-c* and *Pparγ* (Fig. 6C). The decrease in expression levels of these genes indicates that the activity of the lipid synthesis pathway was suppressed. To further explore the lipogenesis signals in liver, we measured AKT1/protein kinase B (PKB) and mammalian target of rapamycin (mTOR) activities, which are the main factors stimulating lipogenesis [40]. Mice with impaired mTORC1 activity have a phenotype similar to that of *lncenc1*-knockout mice. They are lighter, lean, and resistant to weight gain on HFD [41, 42]. As expected, the liver of *lncenc1*$^{3A/3A}$ mice had reduced levels of phosphorylated AKT and mTORC1, suggesting inactivation of the AKT/mTOR

pathway (Fig. 6D). We next examined the expression levels of several essential genes involved in lipogenesis (*CD36*, *Fasn*, *Acc1*, *Srebp1-c*, *Pparγ*, *Gpam*, and *Scd1*) in liver by qPCR. Under HFD conditions, expression levels of lipogenic genes were significantly decreased in *lncenc1*$^{3A/3A}$ mice compared with wild-type mice (Fig. 6E). The gene expression levels were also altered in other major metabolic tissues; *Fasn*, *Pparγ*, and *Scd1* were significantly downregulated in muscle, and *Acc1*, *Srebp1-c, Gpam*, and *Scd1* were significantly downregulated in eWAT of *lncenc1*$^{3A/3A}$ mice on HFD (Fig. 6F). In summary, these analyses suggest that AKT/mTOR-regulated lipogenesis was suppressed in *lncenc1*-knockout mice on HFD. We found an impaired gluconeogenesis in *lncenc1*$^{3A/3A}$ mice, which may be due to the decreased of *Foxo1* transcription level (data wasn't show). This explains both decreased p-AKT and fasting blood glucose level in *lncenc1*-deficient mice.

Based on the metabolic cage experiments, the overall energy expenditure of *lncenc1*-deficient mice under HFD was similar to the WT, although it was increased at a few time points in the night (Fig. S4H). The food intake was not different (Fig. S4I). However, the expression of genes related to energy regulation in brown adipose tissue was slightly increased (Fig. S4G). These results suggested that the increased energy expenditure may contribute to reduced body weight of *lncenc1*-deficient mice after HFD but not the major mechanism. The in-depth mechanisms require further investigation.

### 3.7. Metabolism Disorders of *lncenc1*-Deficient Mice Were of Fetal Origin

We have previously shown that, in mESCs, *lncenc1* promotes the expression of glycolysis-related genes by interacting with RNA-binding proteins HNRNPK and PTBP1 [17]. By analyzing the differentially expressed genes between control and *lncenc1*-depleted mESCs [17], metabolism-implicated pathways such as PI3K-Akt signaling were also affected (Fig. 7A). The expression of *lncenc1* was not detected in metabolism tissues under both NCD and HFD conditions (Fig. S5A), suggesting that

the down-regulated lipogenesis was not caused by *lncenc1* directly. To further explore the developmental origin of impaired glycolysis and AKT/mTOR-regulated lipogenesis, we isolated MEFs from *lncenc1*$^{wt/wt}$ or *lncenc1*$^{3A/3A}$ mouse embryos at embryonic day (E)12.5.

We first tested glycolytic activity. Experiments were performed in primary MEFs under standard culture conditions. The qPCR results showed that 5 of 16 glycolytic genes were significantly downregulated, and the protein levels of TPI1, ALDOC, and PFKP were also clearly decreased in *lncenc1*$^{3A/3A}$ MEFs (Fig. 7B-C). Moreover, glucose uptake and lactate production, the "in" and "out" of glycolysis, were significantly decreased, indicating glycolytic activity was attenuated (Fig. 7D).

Next, we investigated whether *lncenc1* deficiency influenced AKT/mTOR-regulated lipogenesis at an early development stage. We first measured AKT/mTOR pathway activities and found that the levels of phosphorylated AKT and mTORC1 were decreased in *lncenc1* knockdown mESCs (Fig. 7E). It has been reported that this signaling pathway plays a major role in early stages of adipogenesis [43]. Blunting AKT/mTOR signaling inhibits MEF differentiation into adipocytes [44]. To further confirm the activities of AKT/mTOR pathway, we induced MEFs to differentiate into mature adipocytes under standard differentiation conditions with rosiglitazone (Rosi), a high affinity ligand for PPARγ[45, 46](Fig. 7F). The reprogramming of MEFs into adipocytes was impaired in *lncenc1*-depleted mice according to our Oil Red O staining results (Fig. 7F). And there is a lesion in the increase level of mRNA or protein of adipogenesis-related transcription factors (PPARγ, C/EBPα and Srebp1-c) in *lncenc1*$^{3A/3A}$ MEFs during differentiation (Fig. 7G-H). These data indicated that the AKT/mTOR pathway was already affected at an early developmental stage. Although AKT/mTOR signaling is a master regulator of aerobic glycolytic metabolism, it still subjects to reciprocal regulation by growth factors and nutrients such as glucose and amino acids [47, 48]. The glucose starvation impairs the translation of many proteins, including those related to the mTOR pathway

[49]. By comparing the metabolic changes in mice under NCD and HFD conditions, the expression of glycolytic genes decreased in muscle of *lncenc1*-deficient mice with NCD, while the differences became smaller under the HFD condition (Fig. S5D). On the other hand, the mTOR signaling was down-regulated under NCD in liver and eWAT of *lncenc1*-deficient mice (Fig. S5B-C). Furthermore, lipogenic genes had a down-regulated trend in liver and eWAT of NCD *lncenc1*-deficient mice, and the difference between the two genotypes was further enlarged once fed with HFD (Fig. S5E-F).

Based on our previous report [17] and this current study, we propose that *lncenc1* promotes the transcription of glycolytic genes, which maintains cellular energy to activate normal AKT/mTOR signal in early embryos of wild-type mice (Fig. 7I, upper panel); however, *lncenc1* deficiency impairs glycolysis and AKT/mTOR-regulated lipogenesis at an early developmental stage, and this fetal original dysregulation persists in adult mice, presumably through epigenetic mechanisms (Fig. 7I, lower panel).

## 4. DISCUSSION

Metabolic homeostasis is believed to be closely related to many biological processes, such as orderly autophagy occurrence of cells [50] and the normal production of metabolic intermediates [51, 52]. Furthermore, the endocrine signal change[53, 54], alleviated inflammation[55] and anti-aging[56, 57] may contribute to the establishment of new metabolic balance.

In this study, using genetic knockout mouse models, we suggested that depletion of *lncenc1* result in decreased glycolysis and low nutrition condition which further suppress AKT/mTOR-regulated lipogenesis since the embryonic stage[49]. Consistently, *lncenc1* deficiency leads to impaired glucose homeostasis and drives a shift in fuel utilization at weaning. On NCD conditions, in which glucose was the main energy source, *lncenc1*-deficient mice exhibit glucose intolerance and insulin

resistance. Once fed with HFD, *lncenc1*-deficient mice became healthier and resisted to food-induced obesity and disorders due to decreased lipogenesis. Therefore, we proposed that the classical energy homeostasis is impaired in *lncenc1*-deficient mice, and a new metabolic balance is established since the embryonic stage (Fig. 7 I, lower panel).

The “fetal origins of adult disease” hypothesis states that an epigenetic memory of poor fetal and/or infant nutrition causes permanent changes in metabolism, leading to increased risks for chronic metabolic diseases in adult life [5]. The hypothesis has been widely accepted and supported by some epidemiological and genetic research [6, 7]. However, evidence from functional experiments and animal models is still limited and the underlying molecular mechanisms are poorly characterized, since most metabolism genes are ubiquitously expressed and required for normal adult tissue development and physiology. Here, we show that *lncenc1*-knockout mice are suitable models to investigate “fetal origins of adult disease”, due to its embryo-specific expression pattern.

To date, *lncenc1*-deficient mice represent as a metabolic reprogramming model in which the glycolysis and lipogenesis pathways are both impaired since the embryonic stage. It has been reported that *lin28a*- and *lin28b*-deficient mice also exhibit altered glucose metabolism, in part through the let-7-mediated repression of multiple components of the insulin-PI3K-mTOR pathway [8, 58]. However, the effects on glucose and lipid balance were not reported. Recently, functional studies indicated lncRNAs are closely linked to energy metabolism. For example, *Blnc1* interacts with early B-cell factor 2 (EBF2) to promote the differentiation of thermogenic adipocytes [5]; liver-specific *lncLSTR* interacts with TAR DNA-binding protein 43 (TDP-43), a transcriptional repressor, and reduces plasma triglyceride levels [59]; *MUNC* induces MyoD and myogenic gene expression through MyoD-dependent and -independent mechanisms, regulatingmuscle differentiation [60]; a glucagon-producing α cell enriched lncRNA, Paupar, interacts with SR

proteins to promote the alternative splicing of Pax6 and promote α cell development and function[61]. It should be noted that these studies focused on lncRNAs that are expressed in adult tissue, and the potential effects of lncRNA specifically expressed during the embryonic stage on adult energy homeostasis remain largely unknown. Our study provides experimental evidence for the “fetal origins of adult disease” hypothesis and helps in understanding the multiple roles of lncRNAs in metabolism, especially glucose and lipid balance. The sequence of mouse *lncenc1* can be mapped to an intron of human *LINC01331*, but this gene is not expressed in human ES cells. Although *lncenc1* itself is not well-conserved between mouse and human, we expected that the mechanism could be conserved, as many lncRNAs are highly expressed in human ES cells or the human embryo [62].

In this study, we demonstrate that a new metabolic balance of glucose and lipid is established after deletion of *lncenc1*. This study also provides the first piece of data shows that an embryo-expressed lncRNA is required for the adult metabolism homeostasis. However, the mechanism of how the *lncenc1*-dependent abnormal signal in early development is retained as long-lasting memories that can be manifested in adult life is still unclear. Further investigations need to focus on the epigenetic changes on early embryo after disruption of *lncenc1*, and the understanding of upstream regulators and downstream impact that are directly hard-wired into embryo fates. New techniques, such as patch-seq [63], could be powerful tools to reveal in-depth mechanisms including alternative splicing [61], post-translational modifications, degradation [64] and metabolites-mediated epigenome changes [65]. Taken together, our study provides opportunities to understand the physiological roles of embryo-specific lncRNAs in the adult metabolic homeostasis.

**ACKNOWLEDGMENTS**

We thank Yan Tang for assistance with metabolism assays, Yalin Huang for

assistance with fluorescence microscopy and Shanghai Biomodel Organism Co., Ltd for model mouse construction.

**FOUNDING**

This work was supported by the National Key Research and Development Program of China (2018YFC1003500 to B.W.) and the National Natural Science Foundation of China (31601180 to L.C and 31771435 to B.W.).

**Declaration of competing interest**

The authors declare no conflict of interests.

**CRediT authorship contribution statement**

Minzhe Zhu: Conceptualization, Data curation, Formal analysis, Investigation, Resources, Visualization, Writing-original draft, Writing-review & editing. Qianfeng Wang: Data curation, Formal analysis, Investigation, Validation, Writing-review & editing. Pengxiang Tian and Zihao Sun: Data curation, Formal analysis, Investigation. Lu Cheng: Funding acquisition and Investigation. Qi Hong, Pin Lv and Luzhang Ji: Software and Formal analysis. Yang Liu and Qiqun Tang: Methodology, Writing - review & editing. Bo Wen: Conceptualization, Project administration, Funding acquisition, Writing - review & editing and Supervision.

**Appendix A. Supplementary data**

Supplementary data: Table S1-S2.

**References**

1. Goodpaster, B.H. and L.M. Sparks, *Metabolic Flexibility in Health and Disease.* Cell Metab, 2017. **25**(5): p. 1027-1036.
2. Gao, A.W., C. Canto, and R.H. Houtkooper, *Mitochondrial response to nutrient availability and its role in metabolic disease.* EMBO Mol Med, 2014. **6**(5): p. 580-9.

3. Smith, R.L., et al., *Metabolic Flexibility as an Adaptation to Energy Resources and Requirements in Health and Disease.* Endocr Rev, 2018. **39**(4): p. 489-517.
4. Samson, S.L. and A.J. Garber, *Metabolic syndrome.* Endocrinol Metab Clin North Am, 2014. **43**(1): p. 1-23.
5. Barker, D.J., et al., *Weight in infancy and death from ischaemic heart disease.* Lancet, 1989. **2**(8663): p. 577-80.
6. Roseboom, T., S. de Rooij, and R. Painter, *The Dutch famine and its long-term consequences for adult health.* Early Hum Dev, 2006. **82**(8): p. 485-91.
7. van Hoek, M., et al., *Genetic variant in the IGF2BP2 gene may interact with fetal malnutrition to affect glucose metabolism.* Diabetes, 2009. **58**(6): p. 1440-4.
8. Shinoda, G., et al., *Fetal deficiency of lin28 programs life-long aberrations in growth and glucose metabolism.* Stem Cells, 2013. **31**(8): p. 1563-73.
9. Rinn, J.L. and H.Y. Chang, *Genome regulation by long noncoding RNAs.* Annu Rev Biochem, 2012. **81**: p. 145-66.
10. Feyder, M. and L.A. Goff, *Investigating long noncoding RNAs using animal models.* J Clin Invest, 2016. **126**(8): p. 2783-91.
11. Zhao, X.Y. and J.D. Lin, *Long Noncoding RNAs: A New Regulatory Code in Metabolic Control.* Trends Biochem Sci, 2015. **40**(10): p. 586-596.
12. Zhao, X.Y., et al., *A long noncoding RNA transcriptional regulatory circuit drives thermogenic adipocyte differentiation.* Mol Cell, 2014. **55**(3): p. 372-82.
13. Arnes, L., et al., *betalinc1 encodes a long noncoding RNA that regulates islet beta-cell formation and function.* Genes Dev, 2016. **30**(5): p. 502-7.
14. Guttman, M., et al., *lincRNAs act in the circuitry controlling pluripotency and differentiation.* Nature, 2011. **477**(7364): p. 295-300.
15. Perry, R.B. and I. Ulitsky, *The functions of long noncoding RNAs in development and stem cells.* Development, 2016. **143**(21): p. 3882-3894.
16. Rosa, A. and M. Ballarino, *Long Noncoding RNA Regulation of Pluripotency.* Stem Cells Int, 2016. **2016**: p. 1797692.
17. Sun, Z.H., et al., *The Long Noncoding RNA Lncenc1 Maintains Naive States of Mouse ESCs by Promoting the Glycolysis Pathway.* Stem Cell Reports, 2018. **11**(3): p. 741-755.
18. Li, L. and H.Y. Chang, *Physiological roles of long noncoding RNAs: insight from knockout mice.* Trends Cell Biol, 2014. **24**(10): p. 594-602.
19. Li, P., et al., *Germline competent embryonic stem cells derived from rat blastocysts.* Cell, 2008. **135**(7): p. 1299-310.
20. Bao, X., et al., *The p53-induced lincRNA-p21 derails somatic cell reprogramming by sustaining H3K9me3 and CpG methylation at pluripotency gene promoters.* Cell Res, 2015. **25**(1): p. 80-92.
21. Ortega-Molina, A., et al., *Pten positively regulates brown adipose function,*

*energy expenditure, and longevity.* Cell Metab, 2012. **15**(3): p. 382-94.
22. Huang, H., et al., *BMP signaling pathway is required for commitment of C3H10T1/2 pluripotent stem cells to the adipocyte lineage.* Proc Natl Acad Sci U S A, 2009. **106**(31): p. 12670-5.
23. Lee, J., et al., *Withaferin A is a leptin sensitizer with strong antidiabetic properties in mice.* Nat Med, 2016. **22**(9): p. 1023-32.
24. Kim, D., B. Langmead, and S.L. Salzberg, *HISAT: a fast spliced aligner with low memory requirements.* Nat Methods, 2015. **12**(4): p. 357-60.
25. Li, H., et al., *The Sequence Alignment/Map format and SAMtools.* Bioinformatics, 2009. **25**(16): p. 2078-9.
26. Pertea, M., et al., *StringTie enables improved reconstruction of a transcriptome from RNA-seq reads.* Nat Biotechnol, 2015. **33**(3): p. 290-5.
27. Anders, S., P.T. Pyl, and W. Huber, *HTSeq--a Python framework to work with high-throughput sequencing data.* Bioinformatics, 2015. **31**(2): p. 166-9.
28. Love, M.I., W. Huber, and S. Anders, *Moderated estimation of fold change and dispersion for RNA-seq data with DESeq2.* Genome Biol, 2014. **15**(12): p. 550.
29. Ramirez, F., et al., *deepTools2: a next generation web server for deep-sequencing data analysis.* Nucleic Acids Res, 2016. **44**(W1): p. W160-5.
30. Huang da, W., et al., *Extracting biological meaning from large gene lists with DAVID.* Curr Protoc Bioinformatics, 2009. **Chapter 13**: p. Unit 13 11.
31. Wu, J., et al., *The landscape of accessible chromatin in mammalian preimplantation embryos.* Nature, 2016. **534**(7609): p. 652-7.
32. Zhang, Y., et al., *Dynamic epigenomic landscapes during early lineage specification in mouse embryos.* Nat Genet, 2018. **50**(1): p. 96-105.
33. Izumiya, Y., et al., *Fast/Glycolytic muscle fiber growth reduces fat mass and improves metabolic parameters in obese mice.* Cell Metab, 2008. **7**(2): p. 159-72.
34. Ng, J.M., et al., *PET imaging reveals distinctive roles for different regional adipose tissue depots in systemic glucose metabolism in nonobese humans.* Am J Physiol Endocrinol Metab, 2012. **303**(9): p. E1134-41.
35. Zhang, C.S., et al., *Fructose-1,6-bisphosphate and aldolase mediate glucose sensing by AMPK.* Nature, 2017. **548**(7665): p. 112-116.
36. Neel, J.V., *The "thrifty genotype" in 1998.* Nutr Rev, 1999. **57**(5 Pt 2): p. S2-9.
37. Samuel, V.T. and G.I. Shulman, *Nonalcoholic Fatty Liver Disease as a Nexus of Metabolic and Hepatic Diseases.* Cell Metab, 2018. **27**(1): p. 22-41.
38. Donnelly, K.L., et al., *Sources of fatty acids stored in liver and secreted via lipoproteins in patients with nonalcoholic fatty liver disease.* J Clin Invest, 2005. **115**(5): p. 1343-51.
39. Mori, M.A., et al., *Altered miRNA processing disrupts brown/white adipocyte determination and associates with lipodystrophy.* J Clin Invest, 2014. **124**(8): p. 3339-51.

40. Yecies, J.L., et al., *Akt stimulates hepatic SREBP1c and lipogenesis through parallel mTORC1-dependent and independent pathways.* Cell Metab, 2011. **14**(1): p. 21-32.
41. Polak, P., et al., *Adipose-specific knockout of raptor results in lean mice with enhanced mitochondrial respiration.* Cell Metab, 2008. **8**(5): p. 399-410.
42. Chang, G.R., et al., *Rapamycin protects against high fat diet-induced obesity in C57BL/6J mice.* J Pharmacol Sci, 2009. **109**(4): p. 496-503.
43. Carnevalli, L.S., et al., *S6K1 plays a critical role in early adipocyte differentiation.* Dev Cell, 2010. **18**(5): p. 763-74.
44. Zhang, H.H., et al., *Insulin stimulates adipogenesis through the Akt-TSC2-mTORC1 pathway.* PLoS One, 2009. **4**(7): p. e6189.
45. Ardestani, A. and K. Maedler, *Loss of TAZ Boosts PPARgamma to Cope with Insulin Resistance.* Cell Metab, 2020. **31**(1): p. 6-8.
46. El Ouarrat, D., et al., *TAZ Is a Negative Regulator of PPARgamma Activity in Adipocytes and TAZ Deletion Improves Insulin Sensitivity and Glucose Tolerance.* Cell Metab, 2020. **31**(1): p. 162-173 e5.
47. Yuan, T.L. and L.C. Cantley, *PI3K pathway alterations in cancer: variations on a theme.* Oncogene, 2008. **27**(41): p. 5497-510.
48. Yu, J.S. and W. Cui, *Proliferation, survival and metabolism: the role of PI3K/AKT/mTOR signalling in pluripotency and cell fate determination.* Development, 2016. **143**(17): p. 3050-60.
49. Zhang, C.S., D.G. Hardie, and S.C. Lin, *Glucose Starvation Blocks Translation at Multiple Levels.* Cell Metab, 2020. **31**(2): p. 217-218.
50. Bravo-San Pedro, J.M., et al., *Acyl-CoA-Binding Protein Is a Lipogenic Factor that Triggers Food Intake and Obesity.* Cell Metab, 2019. **30**(4): p. 754-767 e9.
51. Chen, S., et al., *Trimethylamine N-Oxide Binds and Activates PERK to Promote Metabolic Dysfunction.* Cell Metab, 2019. **30**(6): p. 1141-1151 e5.
52. Wang, W., et al., *A PRDM16-Driven Metabolic Signal from Adipocytes Regulates Precursor Cell Fate.* Cell Metab, 2019. **30**(1): p. 174-189 e5.
53. Patel, S., et al., *GDF15 Provides an Endocrine Signal of Nutritional Stress in Mice and Humans.* Cell Metab, 2019. **29**(3): p. 707-718 e8.
54. Xie, X., et al., *Activation of Anxiogenic Circuits Instigates Resistance to Diet-Induced Obesity via Increased Energy Expenditure.* Cell Metab, 2019. **29**(4): p. 917-931 e4.
55. Kim, J.D., et al., *Microglial UCP2 Mediates Inflammation and Obesity Induced by High-Fat Feeding.* Cell Metab, 2019. **30**(5): p. 952-962 e5.
56. He, M., et al., *An Acetylation Switch of the NLRP3 Inflammasome Regulates Aging-Associated Chronic Inflammation and Insulin Resistance.* Cell Metab, 2020. **31**(3): p. 580-591 e5.
57. Camell, C.D., et al., *Aging Induces an Nlrp3 Inflammasome-Dependent Expansion of Adipose B Cells That Impairs Metabolic Homeostasis.* Cell

Metab, 2019. **30**(6): p. 1024-1039 e6.
58. Zhu, H., et al., *The Lin28/let-7 axis regulates glucose metabolism.* Cell, 2011. **147**(1): p. 81-94.
59. Li, P., et al., *A liver-enriched long non-coding RNA, lncLSTR, regulates systemic lipid metabolism in mice.* Cell Metab, 2015. **21**(3): p. 455-67.
60. Mueller, A.C., et al., *MUNC, a long noncoding RNA that facilitates the function of MyoD in skeletal myogenesis.* Mol Cell Biol, 2015. **35**(3): p. 498-513.
61. Singer, R.A., et al., *The Long Noncoding RNA Paupar Modulates PAX6 Regulatory Activities to Promote Alpha Cell Development and Function.* Cell Metab, 2019. **30**(6): p. 1091-1106 e8.
62. Breschi, A., T.R. Gingeras, and R. Guigo, *Comparative transcriptomics in human and mouse.* Nat Rev Genet, 2017. **18**(7): p. 425-440.
63. Kravets, V. and R.K.P. Benninger, *From the Transcriptome to Electrophysiology: Searching for the Underlying Cause of Diabetes.* Cell Metab, 2020. **31**(5): p. 888-889.
64. Xiao, Y.Z., et al., *Reducing Hypothalamic Stem Cell Senescence Protects against Aging-Associated Physiological Decline.* Cell Metab, 2020. **31**(3): p. 534-548 e5.
65. Petrus, P., et al., *Glutamine Links Obesity to Inflammation in Human White Adipose Tissue.* Cell Metab, 2020. **31**(2): p. 375-390 e11.

**Figure legends:**

**Figure 1. *lncenc1* is not required for embryonic development and viability**

(A) Expression of *lncenc1* in embryo (E3.5) and somatic tissues under NCD as measured by qRT-PCR. *lncenc1* expression levels were normalized against *Actb*. Results are shown as means ± SEM of triplicates.

(B) Dynamic *lncenc1* expression during early embryo development via RNA-seq.

(C) RNA in situ hybridization (FISH) targeting *lncenc1* in mouse blastocyst stage embryos (E3.5d). POU5F1 was detected by Immunofluorescence. Nuclei were stained with DAPI. Scale bars = 5 μm.

(D) Scheme of two genetic strategies used to knockout *lncenc1* transcription. *lncenc1*$^{3A/3A}$ mice used the premature termination (above) and *lncenc1*$^{\Delta E3/\Delta E3}$ mice complete deleted exon 3 (below).

(E) Expression of *lncenc1* for different genotypes in mouse blastocyst as measured by

qRT-PCR. Expression levels were normalized against *Actb*. Results are shown as means ± SEM of triplicates.

(F) Mendelian inheritance of *lncenc1*$^{3A/3A}$ strain by heterozygote intercrosses. Numbers of observed and expected (in parenthesis) wild type (+/+), heterozygote (+/−) and homozygote (−/−) mice are indicated. Mice were genotyped at d7-d10. Statistical significance of Chi-square Test.

(G) Birth weight for different genotypes of *lncenc1*$^{3A/3A}$ strain. Statistical significance of T-Test.

**Figure 2. *lncenc1* deficiency drives a metabolism change at weaning**

(A) Glucose tolerance test (GTT) for wild type (n = 6) and *Lncenc1*$^{3A/3A}$ (n = 8) at four-week-old. The graph to the right quantifies the area under the curve (AUC).

(B) Serum insulin of wild type (n = 6) and *lncenc1*$^{3A/3A}$ (n = 9) under fasted condition at four-week-old.

(C) The respiratory quotient (RER) measured for wild type and *lncenc1*$^{3A/3A}$ mice at weaning age (n = 5 per genotype). The bar graph at the right side represents the AUC over the indicated 12 hr period. Statistical significance of T-Test: * $p < 0.05$.

(D) Oxygen consumption ($VO_2$) measured for wild type and *lncenc1*$^{3A/3A}$ mice at weaning age (n = 5 per genotype). The bar graph at the right side represents the AUC over the indicated 12 hr period. Statistical significance of T-Test: * $p < 0.05$.

(E-F) Oxygen consumption ($VO_2$), carbon dioxide production ($VCO_2$) and energy expenditure (EE) measured for wild type and *lncenc1*$^{3A/3A}$ mice at weaning age (n = 5 per genotype). The bar graph at the right side represents the AUC over the indicated 12 hr period. Statistical significance of T-Test: * $p < 0.05$.

**Figure 3. *lncenc1*-Deficient Mice have Impaired Glucose Homeostasis Under NCD Conditions**

(A) Weight curves of *lncenc1*$^{3A/3A}$ and littermate wild type mice under NCD (n = 6-10

for each genotype).

(B) Representative images of wild type and *lncenc1*$^{3A/3A}$ mice at 7-month-old.

(C) Cumulative food consumption of *lncenc1*$^{3A/3A}$ and littermate wild type mice under NCD, calculated from the cage average food consumption measured weekly.

(D) Glucose tolerance test (GTT) for wild type (n = 6) and *lncenc1*$^{3A/3A}$ (n = 9) at 12w. Data are shown as mean ± SEM. Statistical significance of T-Test: * $p < 0.05$, ** $p < 0.01$. The graph to the right quantifies the area under the curve (AUC).

(E) Insulin tolerance test (ITT) for wild type (n = 6) and *lncenc1*$^{3A/3A}$ (n = 9) at 15w. Data are shown as mean ± SEM. Statistical significance of T-Test: * $p < 0.05$, ** $p < 0.01$. The graph to the right quantifies the area under the curve (AUC).

(F) Serum insulin levels of *lncenc1*$^{3A/3A}$ and littermate wild type mice under fasted condition (n=6-9 for each genotype).

(G) Determination of BAT, iWAT, eWAT, liver weights *lncenc1*$^{3A/3A}$ and littermate wild type mice (n = 8). Data are shown as mean ± SEM. Statistical significance of T-Test.

(H) Representative images (Scale bars, 1 cm) of BAT, iWAT, eWAT from *lncenc1*$^{3A/3A}$ and littermate wild type mice wild type under NCD.

(I) H&E staining (Scale bars, 100 μm) of BAT, iWAT, eWAT from *lncenc1*$^{3A/3A}$ and littermate wild type mice wild type under NCD.

(J) Adipocyte area of BAT, iWAT, eWAT from *lncenc1*$^{3A/3A}$ and littermate wild type mice wild type under NCD. Data are shown as mean ± SD. Statistical significance of T-Test.

(K) Representative images (Scale bars, 1 cm) of Liver from *lncenc1*$^{3A/3A}$ and littermate wild type mice wild type under NCD.

(L) TG and CHO content in liver of lncenc13A/3A and littermate wild type mice wild type under NCD condition. Data are shown as mean ± SEM. Statistical significance of T-Test.

(M) Representative images (Scale bars, 1 cm), H&E staining (Scale bars, 100 μm) and Oil Red O staining (Scale bars, 200 μm) of liver from *lncenc1*$^{3A/3A}$ and littermate wild type mice wild type under NCD.

(N) Expression of glycolysis genes in muscle of wild type (n = 6) and *lncenc1*$^{3A/3A}$ (n = 7). Data were normalized against *Actb* and are shown as mean ± SEM. Statistical significance of T-Test: * $p < 0.05$.

(O) Protein levels of P-AMPK and AMPK in muscles from wild type and lncenc1$^{3A/3A}$ mice as detected by western blot analysis. ACTB was used as the loading controls.

**Figure 4. Protection from Diet-Induced Obesity in *lncenc1*-Deficent Mice**

(A) Weight curves of *lncenc1*$^{3A/3A}$ and littermate wild type mice under HFD (n = 6-12 for each genotype).

(B) Representative images of *lncenc1*$^{3A/3A}$ and littermate wild type mice at 7-month-old.

(C) Cumulative food consumption of *lncenc1*$^{3A/3A}$ and littermate wild type mice under HFD, calculated from the cage average food consumption measured weekly.

(D) Determination of percentage of fat mass and lean mass of wild type and *lncenc1*$^{3A/3A}$ mice using MRI (n = 5). Data are shown as mean ± SEM. Statistical significance of T-Test: * $p < 0.05$, ** $p < 0.01$, *** $p < 0.001$.

(E) Determination of BAT, iWAT, eWAT, Liver weights from *lncenc1*$^{3A/3A}$ and littermate wild type mice (n = 6). Data are shown as mean ± SEM. Statistical significance of T-Test: * $p < 0.05$, ** $p < 0.01$.

(F and G) Representative images (Scale bars, 1 cm) and H&E staining (Scale bars, 100 μm) of BAT, iWAT, eWAT from *lncenc1*$^{3A/3A}$ and wild type mice under HFD.

(H) Adipocyte area of BAT, iWAT, eWAT from *lncenc1*$^{3A/3A}$ and littermate wild type mice wild type under HFD. Data are shown as mean ± SD. Statistical significance of T-Test.

(I) Representative images (Scale bars, 1 cm) of liver from *lncenc1*$^{3A/3A}$ and wild type mice under HFD.

(J) TG and CHO content in liver of *lncenc1*$^{3A/3A}$ and littermate wild type mice wild type under HFD condition. Data are shown as mean ± SEM. Statistical significance of T-Test.

(K) H&E staining (Scale bars, 100 μm) and Oil Red O staining (Scale bars, 200 μm) of

liver from *lncenc1*$^{3A/3A}$ and littermate wild type mice wild type under HFD.

**Figure 5. Improved metabolic parameters in *lncenc1*-deficent mice**

(A and B) Blood glucose, serum insulin and HOMA-IR levels of *lncenc1*$^{3A/3A}$, *lncenc1*$^{\Delta E3/\Delta E3}$ and their littermate wild type mice under fasted condition (n=6-9 for each genotype).

(C) Glucose tolerance test (GTT) for wild type (n = 8) and *lncenc1*$^{3A/3A}$ mice (n = 8) at 12w. Data are shown as mean ± SEM. Statistical significance of T-Test: * $p < 0.05$, ** $p < 0.01$. The graph to the right quantifies the area under the curve (AUC).

(D) Insulin tolerance test (ITT) for wild type (n = 6) and *lncenc1*$^{3A/3A}$ mice (n = 9) at 15w. Data are shown as mean ± SEM. The graph to the right quantifies the area under the curve (AUC).

(E-G) CHO2I, HDL-C, LDL-C and TRIGL levels in fasted serum of *lncenc1*$^{3A/3A}$, *lncenc1*$^{\Delta E3/\Delta E3}$ and their littermate wild type mice under HFD treatment for 6 months (n=6-8 for each genotype). Data are shown as mean ± SEM. Statistical significance of T-Test: * $p < 0.05$, ** $p < 0.01$.

(H) Expression of lipoprotein lipase (Lpl) in muscle and fat (eWAT) in *lncenc1*$^{3A/3A}$ and their littermate wild type mice under HFD treatment for 6 months (n=5-7 for each genotype). Data are shown as mean ± SEM. Statistical significance of T-Test: * $p < 0.05$.

(I-J) ASTL and ALTL levels in fasted serum of *lncenc1*$^{3A/3A}$, *lncenc1*$^{\Delta E3/\Delta E3}$ and their littermate wild type mice under HFD treatment for 6 months (n=6-8 for each genotype). Data are shown as mean ± SEM. Statistical significance of T-Test: * $p < 0.05$.

**Figure 6. Impaired de novo lipogenesis activity in *lncenc1*-deficent mice**

(A) Heat map of livers from wild type and *lncenc1*$^{3A/3A}$ mice after HFD for 6 months. Data are presented as log2(fold change).

(B) Gene ontology (GO) analysis of up and down-regulated genes (FDR<0.05) in liver of *lncenc1*$^{3A/3A}$ mice after HFD treatment.

(C) Diagram showing the metabolism of FAs in liver. Blue labels represent downregulation in *lncenc1*$^{3A/3A}$ mice.

(D) Relative protein levels in liver from wild type and *lncenc1*$^{3A/3A}$ mice as detected by western blot analysis. β-Actb was used as the loading controls.

(E and F) Relative gene expression in liver (E), muscle and eWAT (F) from wild type and *lncenc1*$^{3A/3A}$ mice under NCD or HFD (n=6-7 for each genotype). Data were normalized against *Actb* and are shown as mean ± SEM. Statistical significance of T-Test: * p < 0.05, ** P<0.01, *** P<0.001

**Figure 7. Metabolism Disorders of *lncenc1*-Deficient Mice Were of Fetal Origin**

(A) Significantly enriched pathways (p < 0.05) of differentially expressed genes upon *lncenc1* knockdown in ES-E14TG2a as revealed by KEGG pathway analysis.

(B) Glycolytic gene expression in wild type and *lncenc1*$^{3A/3A}$ MEFs. (n=4 for each genotype). Data were normalized against *Actb* and are shown as mean ± SEM. Statistical significance of T-Test: * p < 0.05.

(C) Relative protein levels in wild type and *lncenc1*$^{3A/3A}$ MEFs as detected by western blot analysis. β-Actb was used as the loading controls. The graph to the right quantifies the protein levels. Data were shown as mean ± SEM. Statistical significance of T-Test: * p < 0.05.

(D) Measurements of glucose uptake and lactate production in wild type and *lncenc1*$^{3A/3A}$ MEFs (n=3 for each genotype). Data were shown as mean ± SEM. Statistical significance of T-Test: * p < 0.05, ** P<0.01, *** P<0.001.

(E) Relative protein levels upon *lncenc1* knockdown in ES-E14TG2a as detected by western blot analysis. β-Actb was used as the loading controls.

(F) Scheme of reprogramming MEF into adipocyte (above) and representative images during reprogramming and Oil red O staining at day 6 (below) (Scale bars, 200 μm).

(G) PPARγ protein level during reprograming as detected by western blot analysis. ACTB was used as the loading controls.

(H) Lipogenic gene expression during MEFs reprogramming. Values correspond to the mean ± SEM (n = 3 independent MEF preparations per genotype). Statistical significance of T-Test: * p < 0.05, ** P<0.01, *** P<0.001.

(I) Working model of *lncenc1*.

**Figure S1. Genotype identification and characterization of *lncenc1*$^{\Delta E3/\Delta E3}$ strain**

(A and B) Scheme of genotype PCR analysis: *lncenc1*$^{3A/3A}$ mice (A) and *lncenc1*$^{\Delta E3/\Delta E3}$ mice (B). Wild type (WT), heterozygote (HE) and homozygote (HO) mice are indicated.

(C) *lncenc1* expression in the main tissues (liver, fat, muscle) of wildtype control mice and two kinds of knockout mice *lncenc1*$^{3A/3A}$ and *lncenc1*$^{\Delta E3/\Delta E3}$. *lncenc1* expression in embryo as the control. Values correspond to the mean ± SEM (n = 3).

(D) Birth weight for different genotypes of *lncenc1*$^{\Delta E3/\Delta E3}$ strain. Statistical significance of T-Test.

(E) Mendelian inheritance of *lncenc1*$^{\Delta E3/\Delta E3}$ strain by heterozygote intercrosses. Numbers of observed and expected (in parenthesis) wild type (+/+), heterozygote (+/−) and homozygote (−/−) mice are indicated. Mice were genotyped at d7-d10. Statistical significance of Chi-square Test.

**Figure S2. Metabolic characterization of *lncenc1* knockout mice under NCD**

(A) Genes related to energy regulation expression in brown adipose tissue of wild

type and *Incenc1*$^{3A/3A}$ adult mice under the NCD condition (n = 5 per genotype). Statistical significance of T-Test: ** p < 0.01.

(B) Expression of energy expenditure related genes in eWAT under NCD. Values correspond to the mean ± SEM (n = 3).

(C) Expression of fatty acid metabolism genes in liver. Values correspond to the mean ± SEM (n = 3).

(D) The respiratory quotient (RER) measured for wild type and *Incenc1*$^{3A/3A}$ adult mice under the NCD condition (n = 5 per genotype). The bar graph at the right side represents the AUC over the indicated 12 hr period. Statistical significance of T-Test: * p < 0.05.

(E) Physical activity measured for wild type and *Incenc1*$^{3A/3A}$ mice in adult age (n = 6 per genotype) under NCD condition. Data are shown as mean ± SEM.

**Figure S3. Phenotypes of *Incenc1*$^{\Delta E3/\Delta E3}$ mice under the NCD condition**

(A) Weight curves of *Incenc1*$^{\Delta E3/\Delta E3}$ and littermate wild type mice under NCD condition (n = 6-10 for each genotype).

(B) Glucose tolerance test (GTT) for wild type (n = 6) and *Incenc1*$^{\Delta E3/\Delta E3}$ (n = 6) at 12w under NCD condition. Data are shown as mean ± SEM. Statistical significance of T-Test: * p < 0.05, ** p < 0.01.

(C) Insulin tolerance test (ITT) for wild type (n = 6) and *Incenc1*$^{\Delta E3/\Delta E3}$ (n = 6) at 15w under NCD condition. Data are shown as mean ± SEM. Statistical significance of T-Test: * p < 0.05, ** p < 0.01, ***p < 0.001.

(D) Determination of BAT, iWAT, eWAT, liver weights *Incenc1*$^{\Delta E3/\Delta E3}$ and littermate wild type mice (n = 6) under NCD condition. Data are shown as mean ± SEM. Statistical significance of T-Test.

(E) Representative images (Scale bars, 1 cm) of BAT, iWAT, eWAT and liver from *Incenc1*$^{\Delta E3/\Delta E3}$ and littermate wild type mice wild type under NCD.

(F) H&E staining (Scale bars, 100 μm) of BAT, iWAT, eWAT and liver and Oil Red O staining (Scale bars, 200 μm) of liver from *Incenc1*$^{\Delta E3/\Delta E3}$ and littermate wild type mice wild type under NCD.

(G) Adipocyte area of BAT, iWAT, eWAT from *Incenc1*$^{\Delta E3/\Delta E3}$ and littermate wild type mice wild type under NCD. Data are shown as mean ± SD. Statistical significance of T-Test.

(H) Expression of glycolysis genes in muscle of wild type (n = 6) and *Incenc1*$^{\Delta E3/\Delta E3}$ (n = 6) under NCD condition. Data were normalized against *Actb* and are shown as mean ± SEM. Statistical significance of T-Test: * $p < 0.05$

**Figure S4. Phenotypes of *Incenc1*$^{\Delta E3/\Delta E3}$ mice under the HFD condition**

(A) Weight curves of *Incenc1*$^{\Delta E3/\Delta E3}$ and littermate wild type mice under HFD (n = 6-9 for each genotype).

(B) Representative images of *Incenc1*$^{\Delta E3/\Delta E3}$ and littermate wild type mice at 7-month-old.

(C) Determination of BAT, iWAT, eWAT, Liver weights from *Incenc1*$^{\Delta E3/\Delta E3}$ and littermate wild type mice (n=4). Data are shown as mean ± SEM. Statistical significance of T-Test: * $p < 0.05$, ** $p < 0.01$, *** $p < 0.001$.

(D-E) Representative images (Scale bars, 1 cm) , H&E staining (Scale bars, 100 μm) and adipocyte area of BAT, iWAT, eWAT from *Incenc1*$^{\Delta E3/\Delta E3}$ and wild type mice under HFD. Data were shown as mean ± SD.

(F)Representative images (Scale bars, 1 cm), H&E staining (Scale bars, 100 μm) and Oil Red O staining (Scale bars, 200 μm) of liver from *Incenc1*$^{\Delta E3/\Delta E3}$ and wild type mice under HFD.

(G)Genes related to energy regulation in brown adipose tissue in *Incenc1*-deficient mice on HFD. Data are shown as mean ± SEM.

(H) Energy expenditure (EE) measured for wild type and *Incenc1*$^{3A/3A}$ mice in adult age (n = 6 per genotype) under HFD condition. Statistical significance of T-Test: * $p < 0.05$.

(I) Cumulative food consumption of *lncenc1*$^{3A/3A}$ and littermate wild type mice in adult age (n = 6 per genotype) under HFD condition, calculated from the cage average food consumption measured weekly.

**Figure S5. Metabolic changes of *lncenc1* knockout mice.**

(A) *lncenc1* expression in metabolism tissues under NCD and HFD condition, respectively. *lncenc1* expression in embryo as the control. Values correspond to the mean ± SEM (n = 3).

(B) Relative protein levels in wild type and *lncenc1*$^{3A/3A}$ Liver under NCD as detected by western blot analysis. GAPDH was used as the loading controls. The graph to the right quantifies the protein levels. Data were shown as mean ± SEM. Statistical significance of T-Test: * $p < 0.05$, ** $p < 0.01$.

(C)Relative protein levels in wild type and *lncenc1*$^{3A/3A}$ eWAT under NCD as detected by western blot analysis. GAPDH was used as the loading controls. The graph to the right quantifies the protein levels. Data were shown as mean ± SEM. Statistical significance of T-Test.

(D) Expression of glycolysis genes in muscle of wild type(n =6 ) and two knockout strains *lncenc1*$^{3A/3A}$, *lncenc1*$^{\Delta E3/\Delta E3}$ (n = 6) under NCD and HFD condition, respectively.. Data were normalized against *Actb* and are shown as mean ± SEM. Statistical significance of T-Test: * $p < 0.05$.

(E) Expression of lipid metabolic genes in liver of wild type(n = 6) and two knockout strains *lncenc1*$^{3A/3A}$, *lncenc1*$^{\Delta E3/\Delta E3}$ (n = 6) under NCD and HFD condition, respectively.. Data were normalized against *Actb* and are shown as mean ± SEM. Statistical significance of T-Test: * $p < 0.05$.

(F) Expression of lipid metabolic genes in eWAT of wild type(n = 6) and two knockout strains *lncenc1*$^{3A/3A}$, *lncenc1*$^{\Delta E3/\Delta E3}$ (n = 6) under NCD and HFD condition, respectively.. Data were normalized against *Actb* and are shown as mean ± SEM. Statistical significance of T-Test: * $p < 0.05$.

CRediT author statement

**Minzhe Zhu:** Conceptualization, Data curation, Formal analysis, Investigation, Resources, Visualization, Writing-original draft, Writing-review & editing.

**Qianfeng Wang:** Data curation, Formal analysis, Investigation, Validation, Writing-review & editing.

**Pengxiang Tian and Zihao Sun:** Data curation, Formal analysis, Investigation.

**Lu Cheng:** Funding acquisition and Investigation.

**Qi Hong, Pin Lv and Luzhang Ji:** Software and Formal analysis.

**Yang Liu and Qiqun Tang:** Methodology, Writing - review & editing.

**Bo Wen:** Conceptualization, Project administration, Funding acquisition, Writing - review & editing and Supervision.

## Declaration of competing interest

The authors declare that they have no known competing financial interests or personal relationships that could have appeared to influence the work reported in this paper.

**Highlights**

1. Newly weaned mice lacking *Lncenc1*, an embryo-specific lncRNA, have metabolic changes.
2. *Lncenc1*-deficient adult mice show glucose intolerance and insulin resistance under normal chow diet (NCD) conditions.
3. *Lncenc1* deficiency protects mice from high-fat diet (HFD)-induced obesity and associated metabolic dysfunctions.
4. Glycolysis and AKT/mTOR-regulated lipogenesis are repressed in *Lncenc1*-deficient mice and mouse embryonic fibroblasts (MEFs).

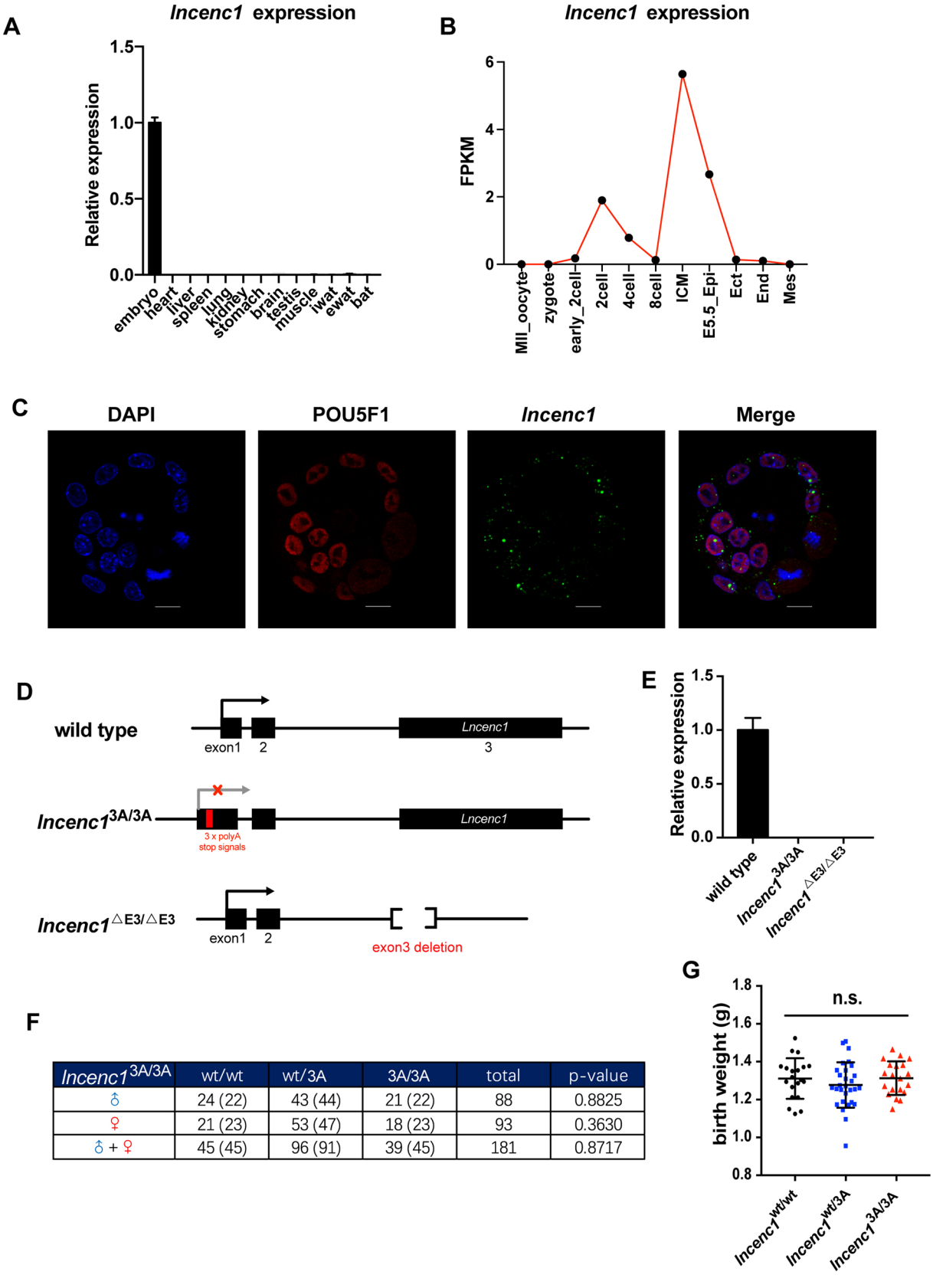


F

| Lncenc1 3A/3A | wt/wt | wt/3A | 3A/3A | total | p-value |
|---|---|---|---|---|---|
| ♂ | 24 (22) | 43 (44) | 21 (22) | 88 | 0.8825 |
| ♀ | 21 (23) | 53 (47) | 18 (23) | 93 | 0.3630 |
| ♂ + ♀ | 45 (45) | 96 (91) | 39 (45) | 181 | 0.8717 |

Figure 1

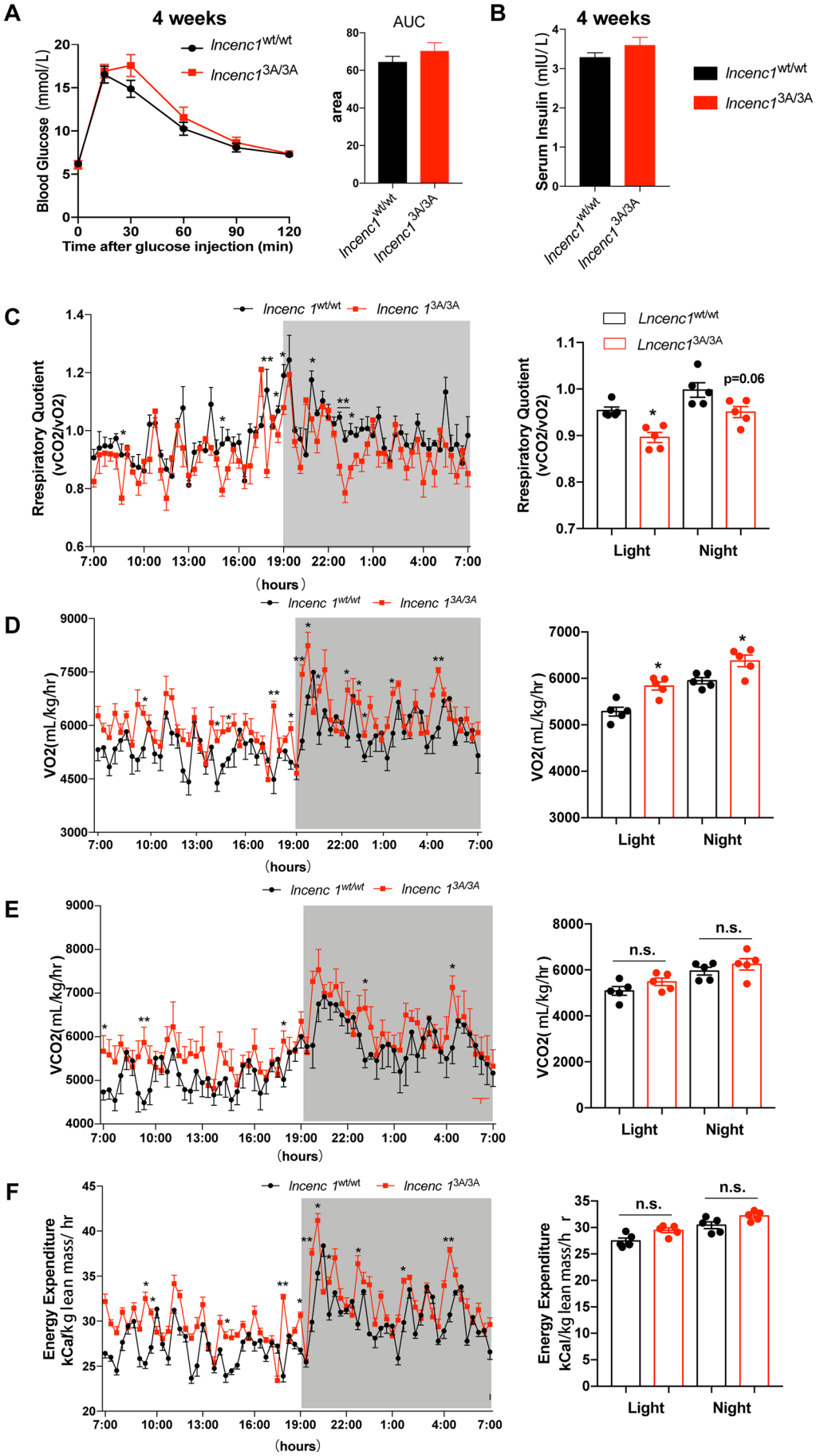
A
4 weeks
Lncenc1wt/wt
Lncenc13A/3A
Blood Glucose (mmol/L)
Time after glucose injection (min)
AUC
area
B
4 weeks
Serum Insulin (mIU/L)
C
Rrespiratory Quotient (vCO2/vO2)
(hours)
p=0.06
Light
Night
D
VO2(mL/kg/hr)
E
VCO2(mL/kg/hr)
n.s.
F
Energy Expenditure kCal/kg lean mass/ hr

Figure 2

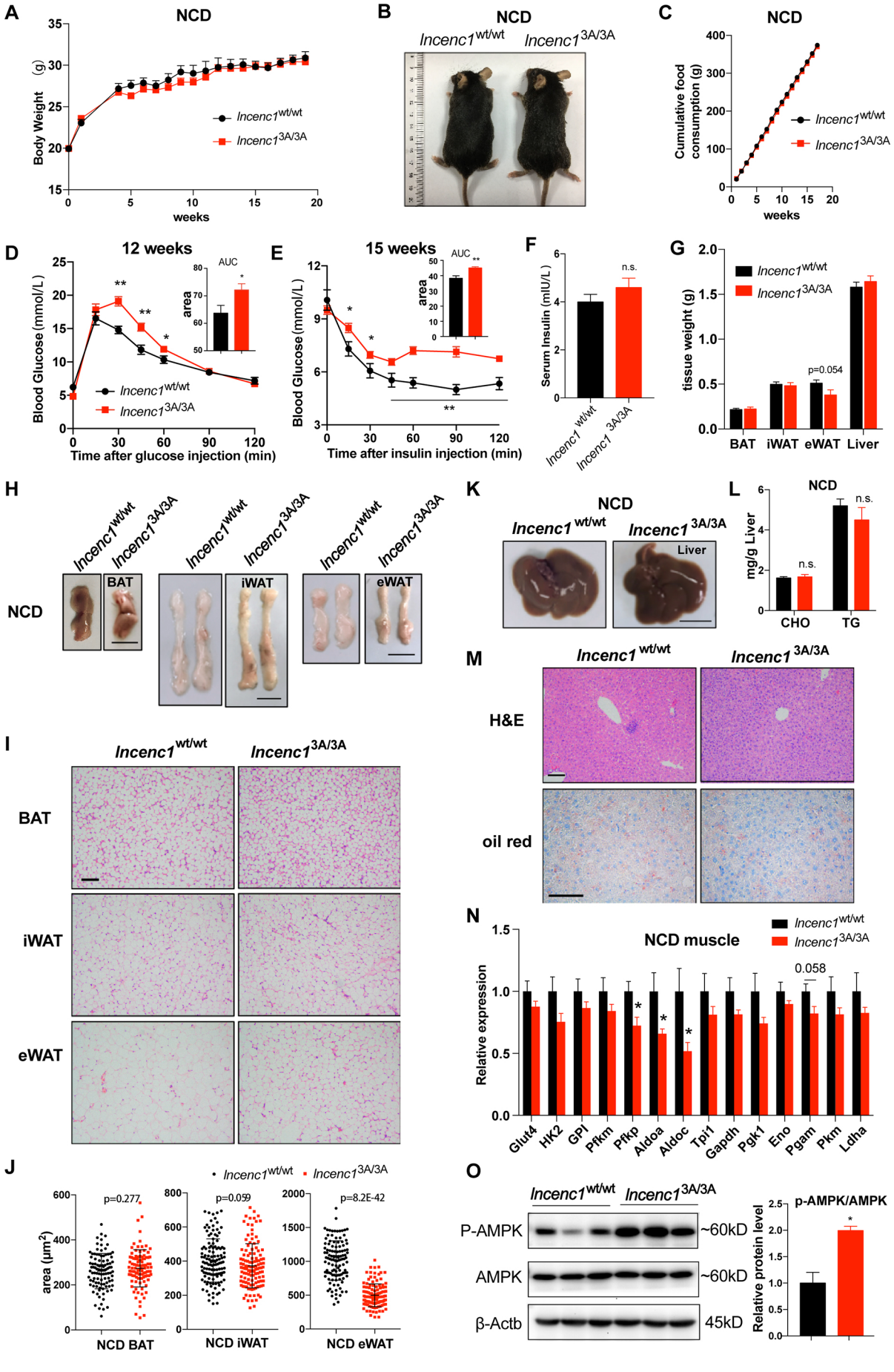
A
NCD
Body Weight (g)
weeks
Incenc1wt/wt
Incenc13A/3A
B
NCD
Incenc1wt/wt
Incenc13A/3A
C
NCD
Cumulative food consumption (g)
weeks
D
12 weeks
Blood Glucose (mmol/L)
AUC
area
Time after glucose injection (min)
E
15 weeks
Blood Glucose (mmol/L)
AUC
area
Time after insulin injection (min)
F
Serum Insulin (mIU/L)
n.s.
G
tissue weight (g)
p=0.054
BAT
iWAT
eWAT
Liver
H
NCD
BAT
iWAT
eWAT
K
NCD
Liver
L
NCD
mg/g Liver
n.s.
CHO
TG
I
BAT
iWAT
eWAT
M
H&E
oil red
N
NCD muscle
Relative expression
0.058
Glut4
HK2
GPI
Pfkm
Pfkp
Aldoa
Aldoc
Tpi1
Gapdh
Pgk1
Eno
Pgam
Pkm
Ldha
J
area (μm2)
p=0.277
p=0.059
p=8.2E-42
NCD BAT
NCD iWAT
NCD eWAT
O
P-AMPK
AMPK
β-Actb
~60kD
~60kD
45kD
p-AMPK/AMPK
Relative protein level

Figure 3

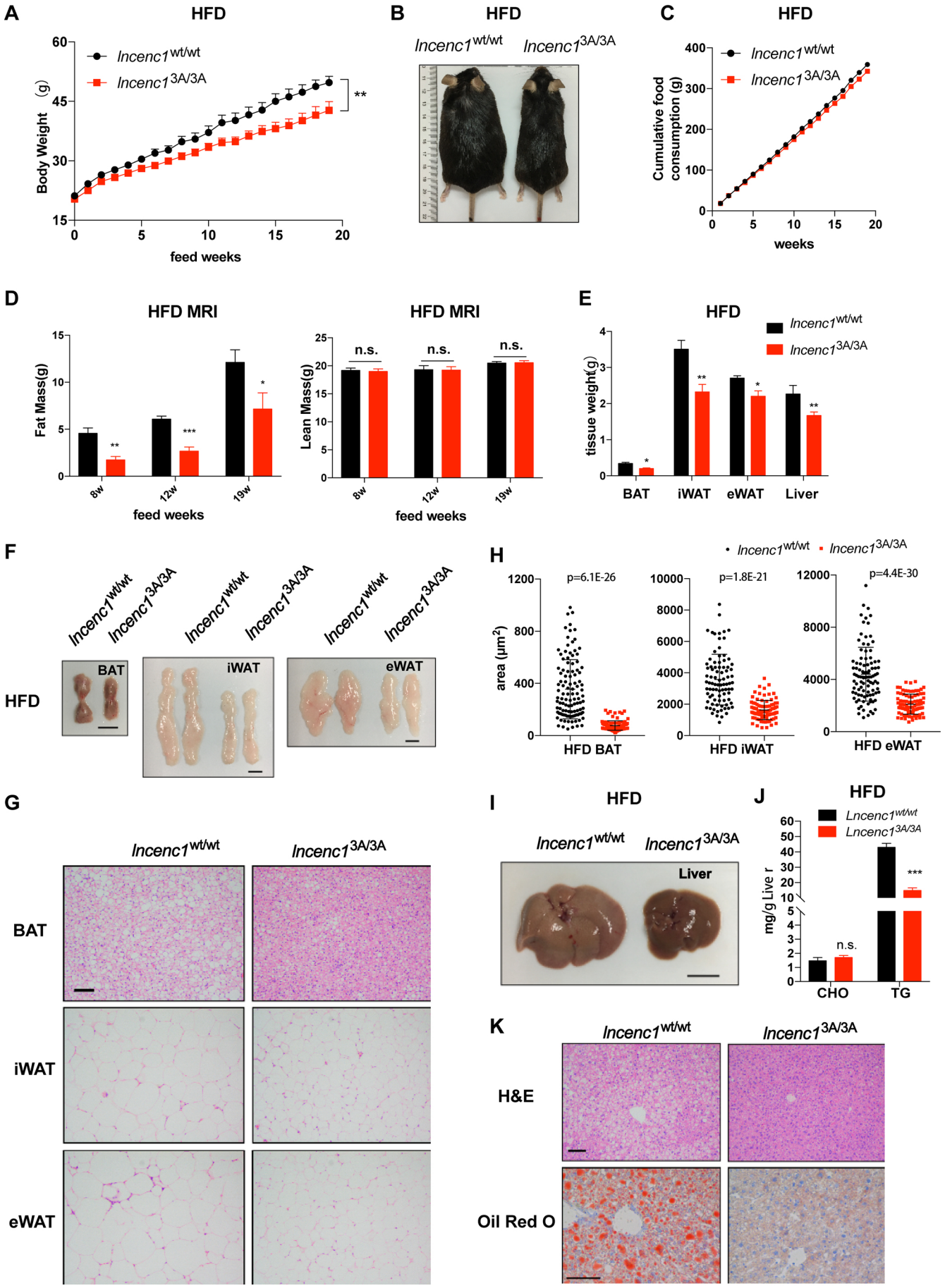
A
HFD
Lncenc1wt/wt
Lncenc13A/3A
Body Weight (g)
feed weeks
**
B
HFD
Lncenc1wt/wt
Lncenc13A/3A
C
HFD
Lncenc1wt/wt
Lncenc13A/3A
Cumulative food consumption (g)
weeks
D
HFD MRI
Fat Mass(g)
feed weeks
8w
12w
19w
HFD MRI
Lean Mass(g)
n.s.
feed weeks
E
HFD
Lncenc1wt/wt
Lncenc13A/3A
tissue weight(g)
BAT
iWAT
eWAT
Liver
F
Lncenc1wt/wt
Lncenc13A/3A
HFD
BAT
iWAT
eWAT
H
Lncenc1wt/wt
Lncenc13A/3A
p=6.1E-26
p=1.8E-21
p=4.4E-30
area (μm2)
HFD BAT
HFD iWAT
HFD eWAT
G
Lncenc1wt/wt
Lncenc13A/3A
BAT
iWAT
eWAT
I
HFD
Lncenc1wt/wt
Lncenc13A/3A
Liver
J
HFD
Lncenc1wt/wt
Lncenc13A/3A
mg/g Live r
n.s.
***
CHO
TG
K
Lncenc1wt/wt
Lncenc13A/3A
H&E
Oil Red O

Figure 4

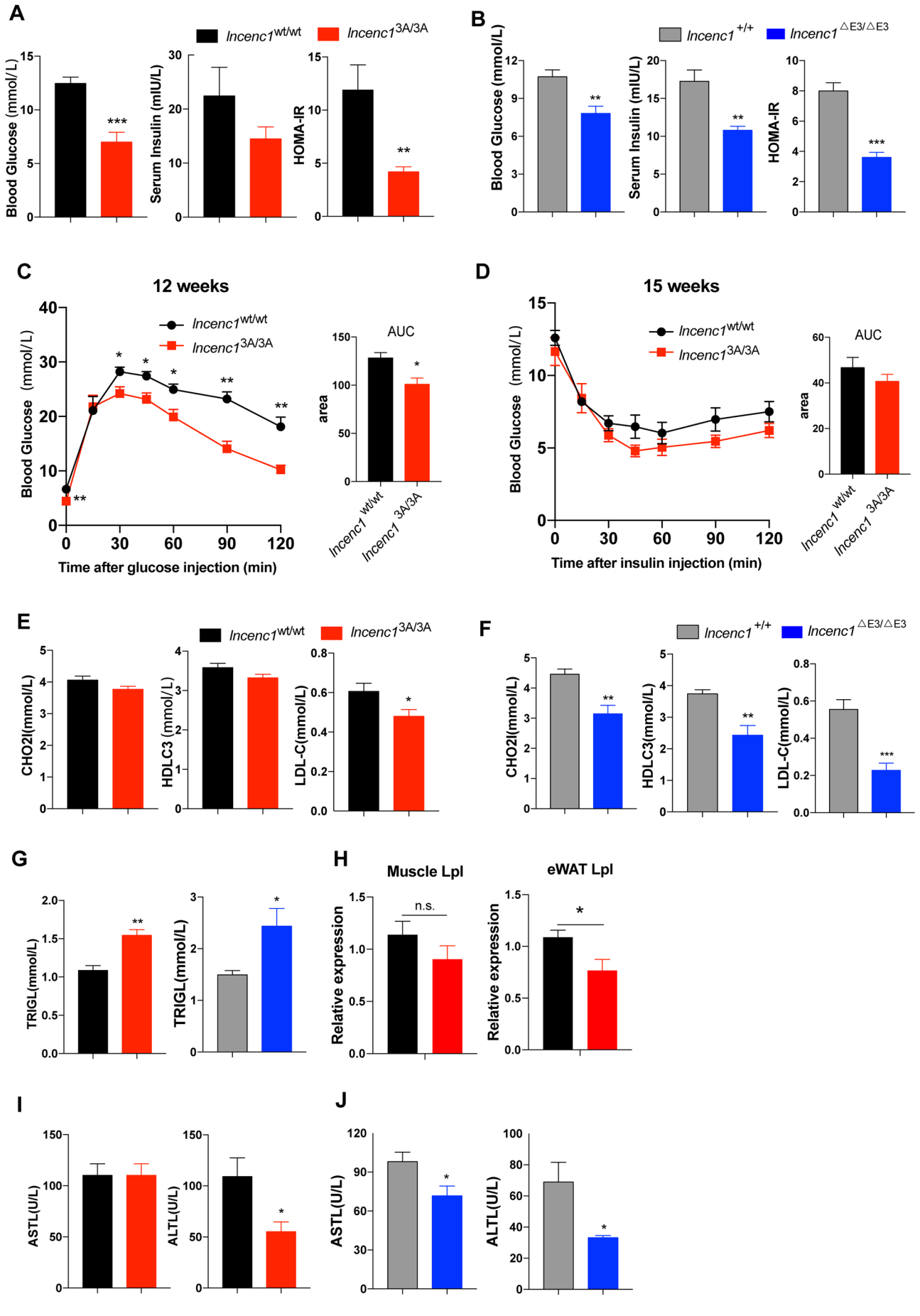
A
Incenc1wt/wt
Incenc13A/3A
Blood Glucose (mmol/L)
Serum Insulin (mIU/L)
HOMA-IR
B
Incenc1+/+
Incenc1△E3/△E3
C
12 weeks
Time after glucose injection (min)
AUC
area
D
15 weeks
Time after insulin injection (min)
E
CHO2l(mmol/L)
HDLC3 (mmol/L)
LDL-C(mmol/L)
F
HDLC3(mmol/L)
G
TRIGL(mmol/L)
H
Muscle Lpl
eWAT Lpl
Relative expression
n.s.
I
ASTL(U/L)
ALTL(U/L)
J

Figure 5

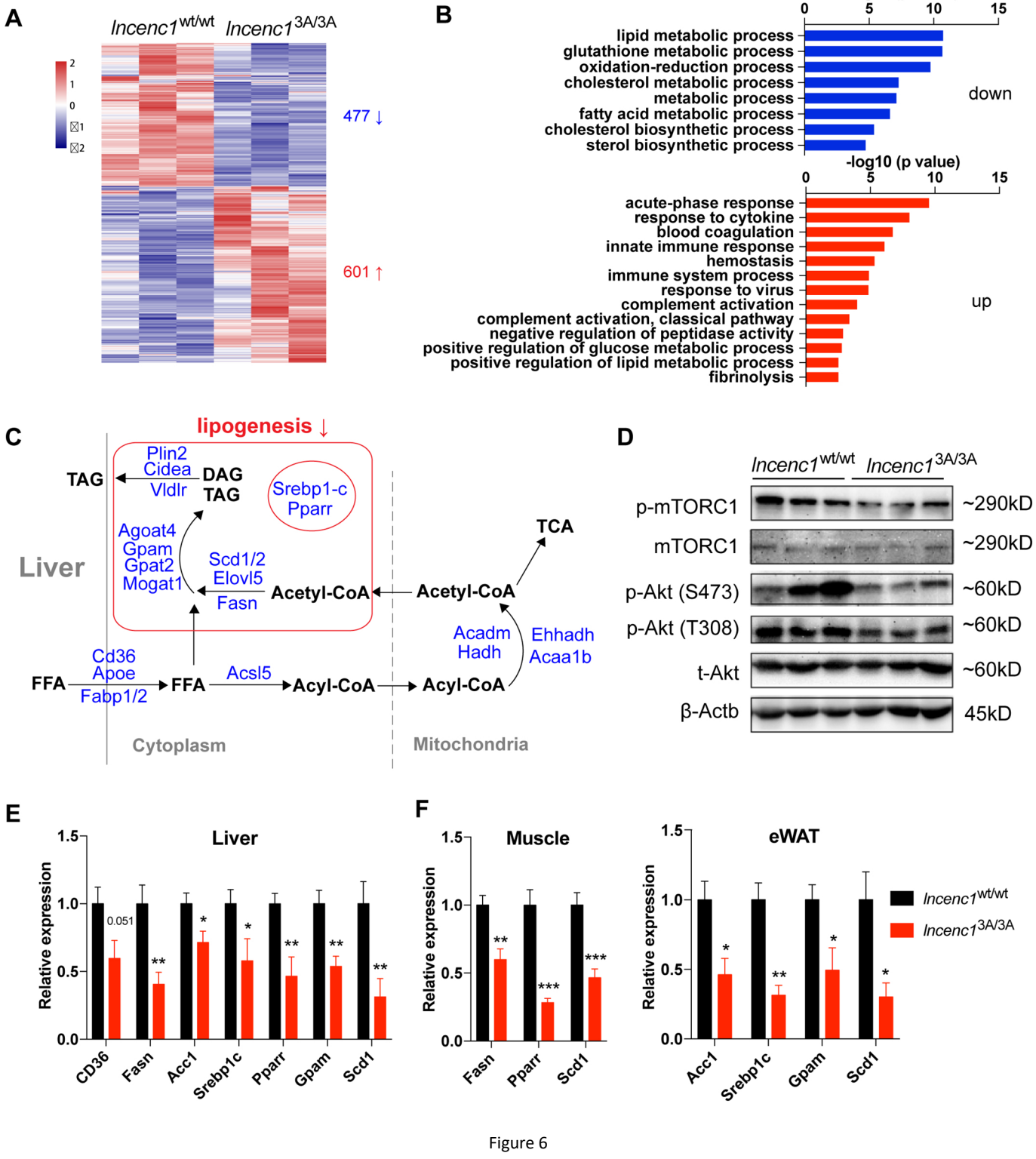
A
Incenc1wt/wt
Incenc13A/3A
477 ↓
601 ↑
B
-log10 (p value)
lipid metabolic process
glutathione metabolic process
oxidation-reduction process
cholesterol metabolic process
metabolic process
fatty acid metabolic process
cholesterol biosynthetic process
sterol biosynthetic process
down
acute-phase response
response to cytokine
blood coagulation
innate immune response
hemostasis
immune system process
response to virus
complement activation
complement activation, classical pathway
negative regulation of peptidase activity
positive regulation of glucose metabolic process
positive regulation of lipid metabolic process
fibrinolysis
up
C
lipogenesis ↓
Liver
TAG
Plin2
Cidea
Vldlr
DAG
TAG
Srebp1-c
Pparr
Agoat4
Gpam
Gpat2
Mogat1
Scd1/2
Elovl5
Fasn
Acetyl-CoA
TCA
Acadm
Hadh
Ehhadh
Acaa1b
Cd36
Apoe
Fabp1/2
FFA
Acsl5
Acyl-CoA
Cytoplasm
Mitochondria
D
Incenc1wt/wt
Incenc13A/3A
p-mTORC1
mTORC1
p-Akt (S473)
p-Akt (T308)
t-Akt
β-Actb
~290kD
~290kD
~60kD
~60kD
~60kD
45kD
E
Liver
Relative expression
CD36
Fasn
Acc1
Srebp1c
Pparr
Gpam
Scd1
F
Muscle
eWAT
Incenc1wt/wt
Incenc13A/3A

Figure 6

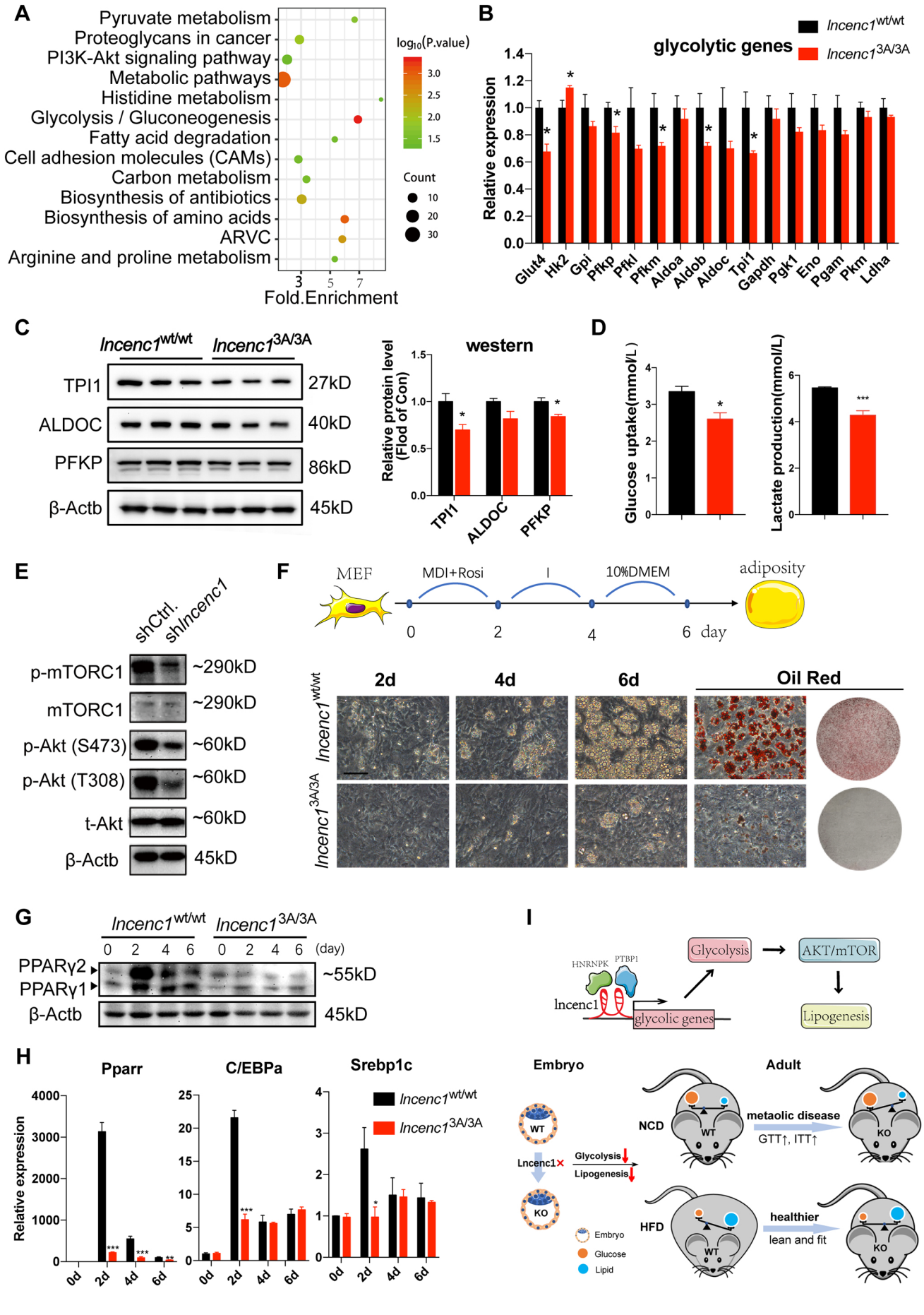
A
Pyruvate metabolism
Proteoglycans in cancer
PI3K-Akt signaling pathway
Metabolic pathways
Histidine metabolism
Glycolysis / Gluconeogenesis
Fatty acid degradation
Cell adhesion molecules (CAMs)
Carbon metabolism
Biosynthesis of antibiotics
Biosynthesis of amino acids
ARVC
Arginine and proline metabolism
log10(P.value)
Count
Fold.Enrichment
B
glycolytic genes
Incenc1wt/wt
Incenc13A/3A
Relative expression
Glut4 Hk2 Gpi Pfkp Pfkl Pfkm Aldoa Aldob Aldoc Tpi1 Gapdh Pgk1 Eno Pgam Pkm Ldha
C
Incenc1wt/wt
Incenc13A/3A
TPI1 27kD
ALDOC 40kD
PFKP 86kD
β-Actb 45kD
western
Relative protein level (Flod of Con)
TPI1 ALDOC PFKP
D
Glucose uptake(mmol/L)
Lactate production(mmol/L)
E
shCtrl. shIncenc1
p-mTORC1 ~290kD
mTORC1 ~290kD
p-Akt (S473) ~60kD
p-Akt (T308) ~60kD
t-Akt ~60kD
β-Actb 45kD
F
MEF
MDI+Rosi
I
10%DMEM
adiposity
0 2 4 6 day
2d 4d 6d Oil Red
Incenc1wt/wt
Incenc13A/3A
G
Incenc1wt/wt
Incenc13A/3A
0 2 4 6 0 2 4 6 (day)
PPARγ2
PPARγ1
~55kD
β-Actb 45kD
I
HNRNPK PTBP1
lncenc1
glycolic genes
Glycolysis
AKT/mTOR
Lipogenesis
H
Pparr
C/EBPa
Srebp1c
Incenc1wt/wt
Incenc13A/3A
Relative expression
0d 2d 4d 6d
Embryo
Adult
WT
Lncenc1×
KO
Glycolysis↓
Lipogenesis↓
Embryo
Glucose
Lipid
NCD
metaolic disease
GTT↑, ITT↑
HFD
healthier
lean and fit

Figure 7